Supporting Information

Electrochemically grafted molecular layers as on-chip energy storage molecular junctions

Rajwinder Kaur[a,≠], Ankur Malik[a,≠], Ritu Gupta[a], Kusum Kumari[b], Saurabh Kumar Singh[b], Paulo Roberto Bueno[c] and Prakash Chandra Mondal[a,*]

[a]Department of Chemistry, Indian Institute of Technology Kanpur, Uttar Pradesh 208 016, India

[b]Department of Chemistry, Indian Institute of Technology Hyderabad, Kandi, Telangana 502 285, India.

[c]Department of Engineering, Physics and Mathematics, Institute of Chemistry, Sao Paulo State University (UNESP), CEP. 14800-060, Sao Paulo, Brazil.

[≠]These two authors equally contributed to this work.

E-mail: pcmondal@iitk.ac.in (P.C.M.)

Contents

1a. Reagent, Materials and methods

5-amino-2-mercaptobenzimidazole (98%), tetrafluoroboric acid (HBF_4, 48% in water), sodium nitrite (97%, $NaNO_2$), tetrabutylammonium tetrafluoroborate (99%, $TBABF_4$), tetrabutylammonium hexafluorophosphate (99%, $TBAPF_6$), and tetrabutylammonium perchlorate (99%, $TBAClO_4$) were purchased from Sigma-Aldrich (Bangalore, India), hydrochloric acid (Finar), acetonitrile (Avantore, HPLC-grade) were used as received. Hydrogen peroxide (30% w/v) was purchased from Finar Chemicals. $AgNO_3$ (99.8%) and sulphuric acid (18 M, 98%) were purchased from Rankem Chemicals. Various solvents including hexane, iso-propyl-alcohol, and acetone were purchased from Finar Chemicals. 2 cm ×1.5 cm quartz substrates were obtained from Ossila Ltd., Sheffield, UK. ITO, Al, and Au targets were purchased from Kurt J. Lesker Company. Indium-tin oxide-coated glass substrates (ITO, thickness: 1.1 mm, sheet resistance: <17 Ωsq^{-1}) were purchased from Nanoshel. A Pt wire used as a counter electrode and an Ag wire reference electrode were purchased from Metrohm. The reference electrode used during the measurements was composed of Ag wire immersed in the solution of 0.01 M $AgNO_3$ and 0.1 M electrolyte ($TBABF_4$) in acetonitrile.

For characterization purposes, commercial ITO electrodes (2.5 cm × 1 cm) were cleaned in hexane, acetone, and isopropyl alcohol in sequence by ultra-sonication for 15 minutes each to eliminate traces of organic contaminants. Cleaned ITO substrates were dried using an N_2 gun, followed by heating in an oven at 100°C for 30 minutes to remove any traces of water or organic solvent. Before bottom electrode deposition, the quartz substrates were dipped into piranha solution (H_2SO_4:H_2O_2 = 3:1, 24 mL) for 30 minutes followed by sonication and washing with a copious amount of D.I. water (18.2 MΩ) and dried at 100 °C overnight. Around 100 nm Au deposited on a 5 nm Cr adhesive layer on cleaned glass substrates utilized for Raman spectroscopy was prepared by an electron-beam evaporation.

1b. Instrumentations.

^1H NMR spectrum was recorded on a JEOLECX 500 FT (500 MHz) at 298 K and the NMR peak positions are listed with reference to tetramethylsilane (TMS). The UV-vis spectra (both solution-phase and thin film) were recorded on the JASCO UV-Visible-NIR V-770 spectrophotometer (equipped with tungsten lamp for visible range and deuterium lamp for ultraviolet range) in the 300-800 nm range using bandwidth 2 nm. Electrochemical grafting of the molecular layers of varied thicknesses and solution phase electrochemical impedance spectroscopy measurements for different electrolytes were performed on a Metrohm Autolab electrochemical workstation (AUT204, FRA32M.S PGSTAT204 with FRA32M module). After electrochemical grafting of the molecular layers, films were immediately transferred to the vacuum chamber to minimize contamination by air. Fourier-transform Infrared spectra (FT-IR) were

measured using a Bruker Optik GmbH Alpha II spectrophotometer equipped with a standard source MIR and an RT-DLATGS detector. The thin film FTIR spectra were collected in ATR mode by placing the ITO/BENZ sample on ZnSe crystal in the frequency range of 4000 - 600 cm^{-1} with a spectral resolution of 4 cm^{-1} over 100 scans. The water vapor and carbon dioxide were subtracted from the spectra. Finally, the baseline correction and peak fitting analysis of all spectra were performed using OPUS 8.1 software. Raman spectra were recorded using a confocal Raman microscope equipped with an air-cooled solid-state laser (λ = 532 nm) and a CCD camera. The excitation laser radiation was coupled into a microscope through a single-mode optical fiber with a 40 mm diameter. A Princeton Instruments Acton Spectra Pro 2500 and objective lens 50X were used. Raman scattered light was focused on a multi-mode fiber (40 mm diameter) and monochromator with a 600 line/mm grating. Raman data were accumulated through laser power (40 mW), and spectra were collected using 20 scans with an integration time of 2 s. The spectrometer monochromator was calibrated using the Raman scattering line of naphthalene (1382 cm^{-1}). The commercial Asylum Research (Oxford Instruments) was used to conduct the AFM analysis, and a silicon probe with a force constant of 0.5 N m^{-1} was used. Images were captured at a scan rate of 0.70 Hz, with a set point in the range of 0.25 V to 0.35 V, and a scan area of 1 μm × 1 μm. XPS spectra were collected on PHI5000 Versa Probe-III (Physical Electronic) spectrometer using Al Kα radiation (1486.6 eV). The obtained data were analyzed using origin software using a Gaussian line shape. The individual XPS spectra were calibrated with respect to C 1s main peak 284.8 eV. Pan Analytical X'pert Power X-Ray Diffractometer operating with an X-ray Source Cu Kα (λ =1.54056 Å) was utilized for accruing the thin film XRD data. The XRD was recorded in 5-90° 2 theta range at a scan rate of 2° min^{-1}. The ATS 500 PDC Magnetron sputtering system was utilized for ITO deposition. Al top electrode was deposited via thermal evaporation method using Hind High Vac HVV BC 300. E-beam deposition 100 nm Au electrodes were made on a Hind High Vacuum deposition, (Bangalore, India) system. A Keithley Source meter 2604B was used for I-V (current-voltage) measurements. Hall effect studies were performed using a Tabletop Hall effect measurement system equipped with a permanent magnet of 0.5 ± 0.03 Tesla magnetic field strength and sample holder model number- SPCB-21. Electrochemical impedance spectroscopy (EIS) measurements were performed using a GAMRY Reference 600+ potentiostat for solid-state ITO/Al and ITO/BENZ/Al MJs of varying thicknesses using the set up employed for I-V measurements (**Figure S11b**).

2. Synthesis and characterization of diazonium salt of 5-amino-2-mercaptobenzimidazole

(a) Synthesis of diazonium salt

To a 3 mM (496 mg) solution of 5-amino-2-mercaptobenzimidazole in 2 mL ethanol taken in a two-neck round-bottom flask (RB) equipped with a small magnetic stir bar, 2 mL of concentrated HCl was added dropwise. The reaction mixture was cooled to -5°C with the help of a NaCl/ice bath. An ice-cold aqueous solution of $NaNO_2$ (6 mM, 414 mg in 2 mL D.I.) was added very slowly to the reaction mixture while maintaining the temperature below 0°C with constant stirring, which continued for another 30 minutes after the addition of $NaNO_2$. Then 2 mL of concentrated HBF_4 (48 wt%) was added dropwise and stirred for 5 h while maintaining the temperature of the reaction mixture below 0°C (**Scheme 1**). The bright yellow solid product was vacuum filtered, and washed with copious amounts of cold diethyl ether. The product was labeled as BENZ-D and stored at -4°C.[1]

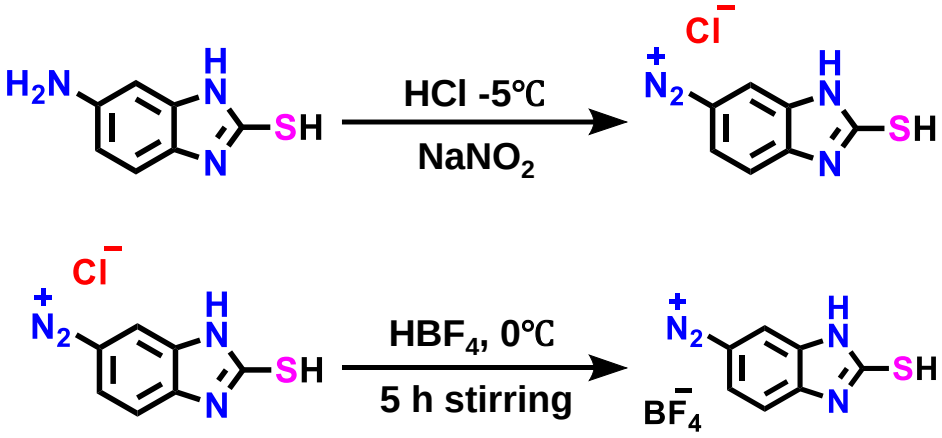

Scheme 1. Synthesis of diazonium salt of 5-amino-2-mercaptobenzimidazole.

(b) Characterization of diazonium salt

The BENZ-D salt was characterized by various spectroscopic techniques. ^{1}H NMR (500 MHz, ACETONITRILE-D3): δ 11.11 (s, 1H), 10.84 (s, 1H), 8.20 (d, J = 6.8 Hz, 1H), 8.11 (s, 1H), 7.50 (d, J = 8.9 Hz, 1H) (**Figure S1**).

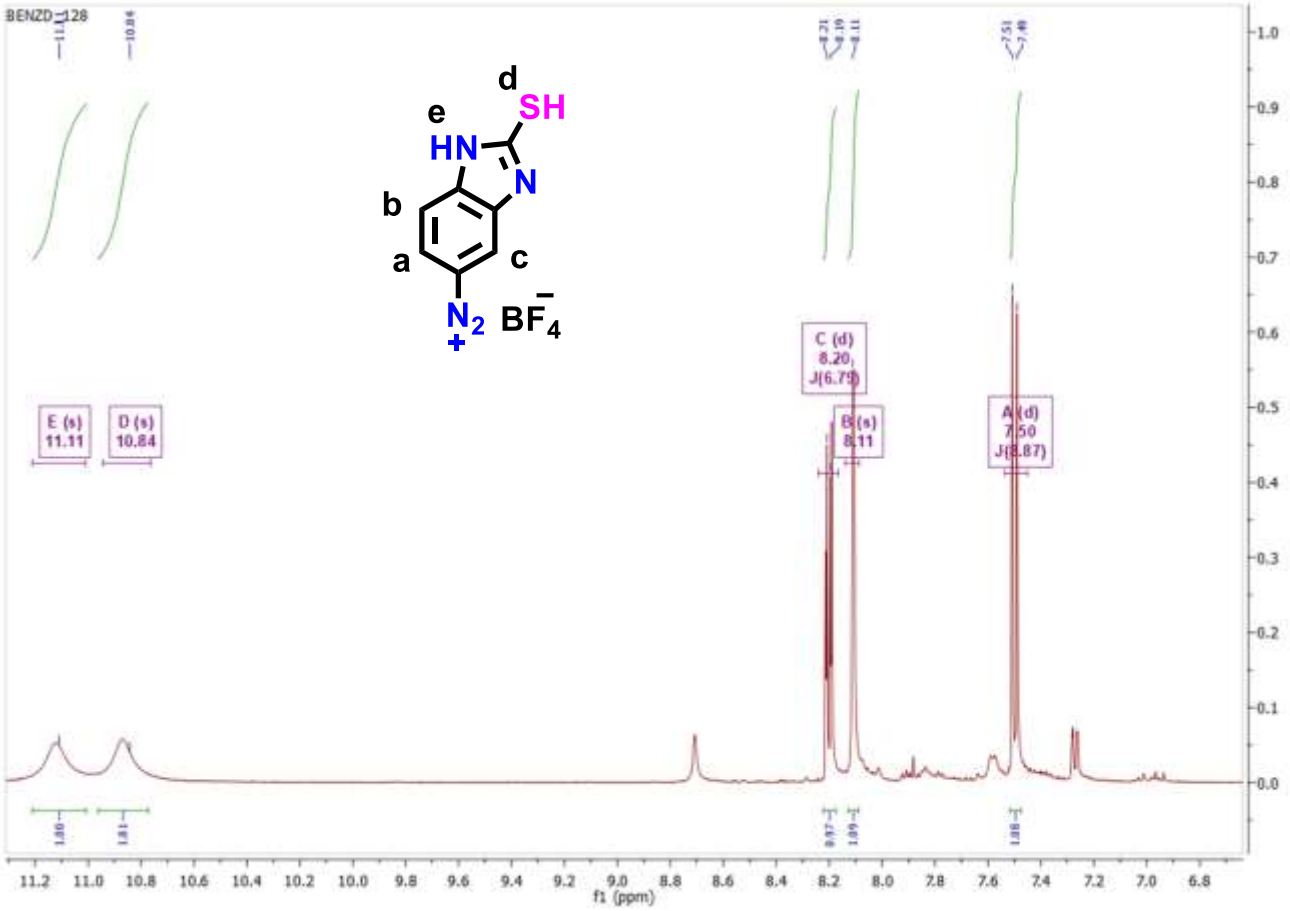

Figure S1. ^{1}H NMR spectrum of BENZ-D diazonium salt in CD_3CN. The ^{1}H NMR peak positions are assigned with reference to tetramethylsilane (TMS).

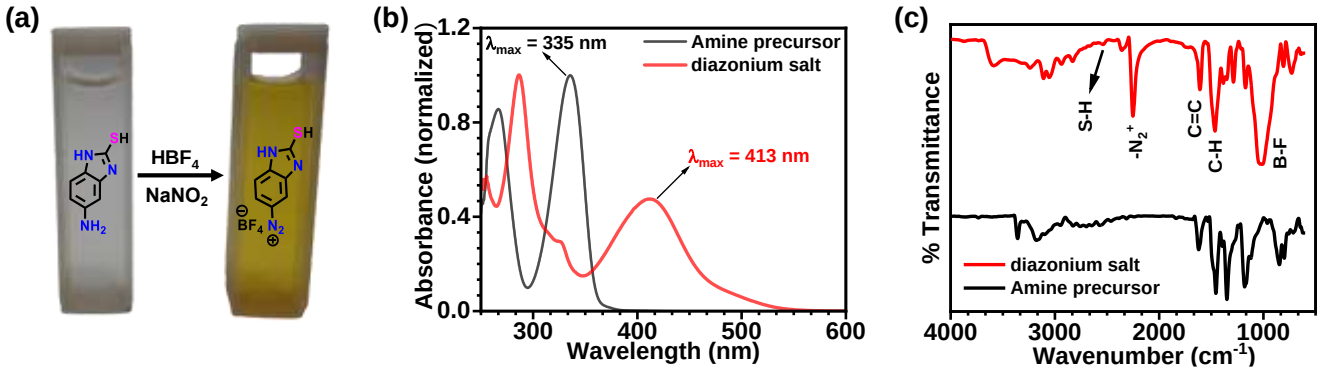

Figure S2. Conversion of 5-amino-2-mercaptobenzimidazole to corresponding diazonium salt (a) change in color from offwhite to yellow upon diazotization of 5-amino-2-mercaptobenzimidazole (b) UV-Visible spectra, and (c) FTIR-spectra illustrating the conversion of amine moiety to diazo group in 5-amino-2-mercaptobenzimidazole.

3. ITO bottom electrode patterning on quartz substrates:

The bottom electrode shadow mask having a width of 0.5 mm (500 µm) was placed on cleaned quartz substrates and 100 nm ITO was deposited by PDC Magnetron sputtering. Before the ITO bottom electrode deposition, the sputtering chamber was pumped to a pressure of 1.56 $\times 10^{-3}$ mbar. ITO electrodes were deposited using a 4-inch diameter ITO target of 99.9% purity. During the deposition, the Argon gas flow rate was kept at 15 sccm using a mass flow controller to maintain the chamber pressure, and power to the sputtering gun was maintained at 30 W (**Figure S3**).

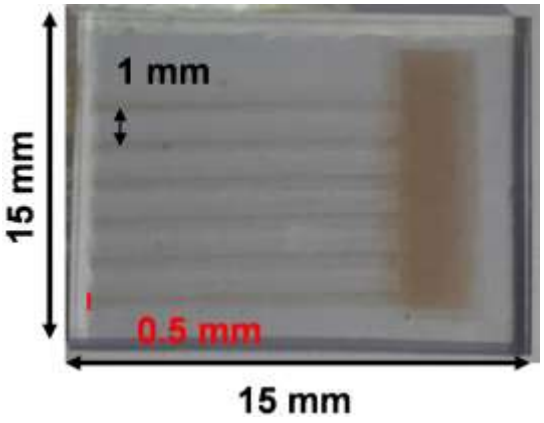

Figure S3. Digital photograph of patterned ITO on the quartz substrate.

4a. Electrochemical grafting of diazonium salt

An electrochemical grafting technique was employed to grow molecular thin films/layers of 2-mercaptobenezimidazole on ITO electrodes. For this purpose, 4 mM diazonium salt BENZ-D (**Scheme S1**) solution in acetonitrile along with 0.1 M tetrabutylammonium tetrafluoroborate ($TBABF_4$) as supporting electrolyte was taken in an electrochemical cell. A conventional three-electrode electrochemical set-up having ITO as the working electrode, $Ag/AgNO_3$ reference electrode, and Pt wire as the counter electrode was utilized to electrochemically deposit molecular thin films employing cyclic voltammetry technique. Electroreduction of diazonium salt was performed by sweeping the working electrode potential from 0 V to -0.85 V (vs. $Ag/AgNO_3$) at a scan rate of 0.1 V s^{-1}. A dominant cathodic peak at -0.64 V was observed in the first cycle but not in the rest of the cycles (**Figure S4**), which stated that aryl radical reaction is a very fast process.[2] Surface coverage was calculated using the well-established formula given in equation (1),

$$\Gamma = \frac{Q}{nFA} \quad \text{……..(i)}$$

Where Q is the charge obtained by integrating the first grafting CV cycle, F is the Faraday constant, n is the number of electrons transferred in the diazonium reduction process (here n = 1), A is the effective area of the working electrode, Γ is surface coverage of grafted species in mol cm^{-2} (**Table S1**).[3]

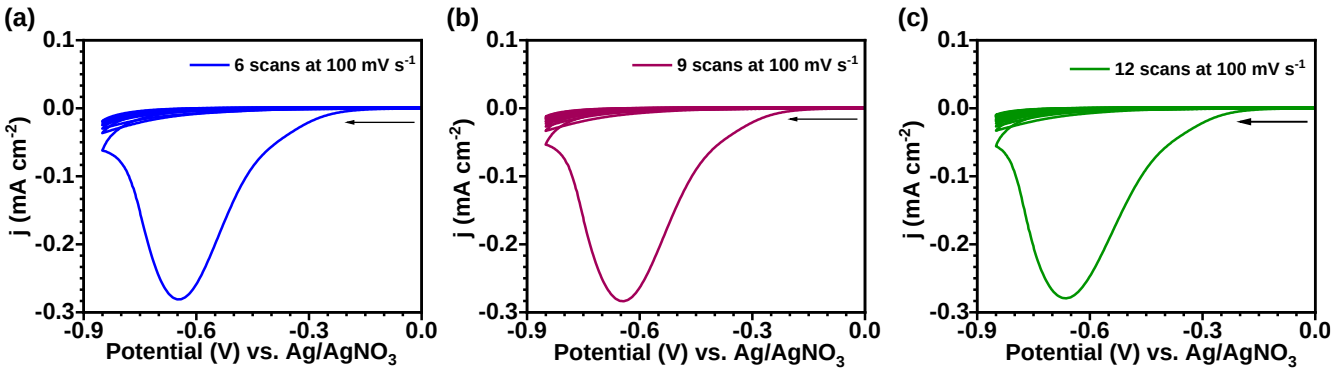

Figure S4. Cyclic voltammogram of electrochemically grafted BENZ molecular layers on commercial ITO electrodes (a) Film-1, (b) Film-2, and (c) Film-3. $Ag/AgNO_3$ and Pt wire were used as reference and counter electrodes respectively.

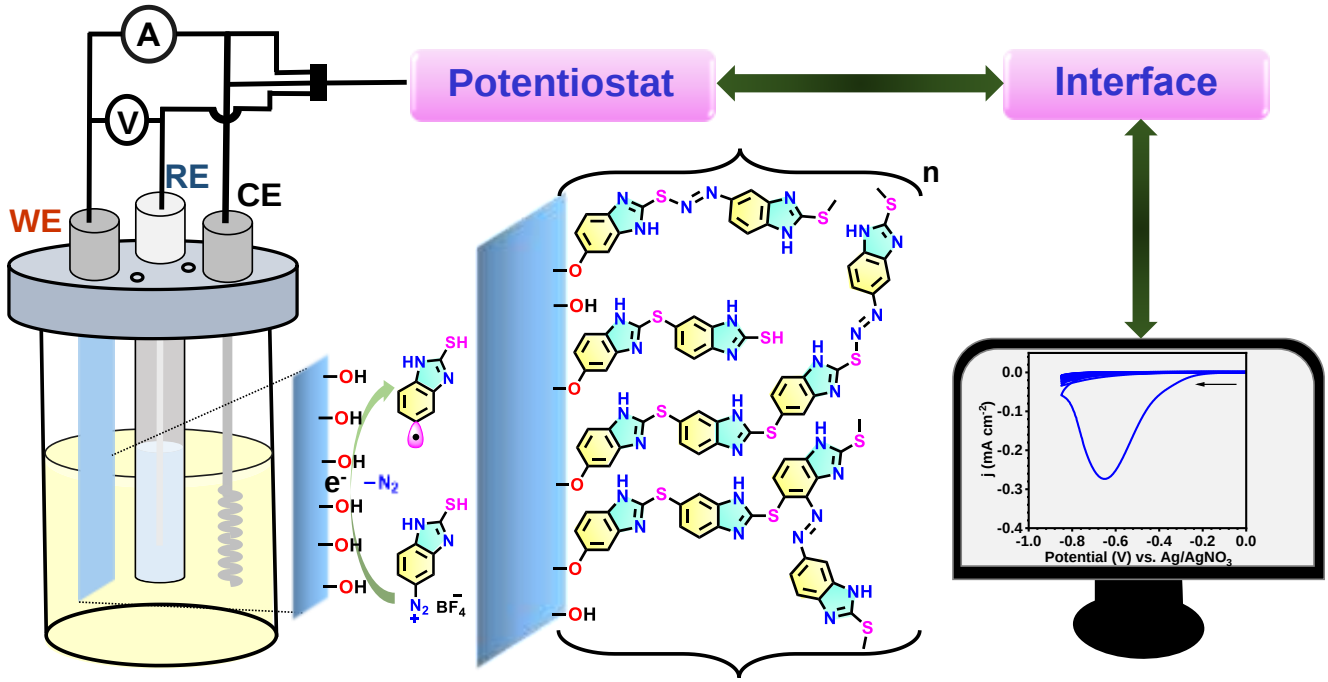

Figure S5. Three electrode set-up for electrochemical grafting of BENZ-D layers on ITO (working) electrode using 4 mM diazonium solution and 0.1 M $TBABF_4$ in acetonitrile. $Ag/AgNO_3$ and Pt wire were utilized as reference and counter electrodes respectively. Inset shows the plausible layer growth on -OH terminated ITO electrode.

Table S1. Electrochemical grafting parameters and surface coverage of Film 1-3.

S.N.	Sample	CV cycles	Surface Coverage (mol cm^{-2})	Thickness from AFM (nm)
1.	Film-1	6	$6.1 \pm 0.3 \times 10^{-9}$	10.0 ± 1.8
2.	Film-2	9	$6.3 \pm 0.5 \times 10^{-9}$	14.3 ± 2.9
3.	Film-3	12	$6.5 \pm 0.4 \times 10^{-9}$	18.6 ± 0.9

A similar E-Chem grafting process was followed using patterned ITO on a quartz substrate as a working electrode for device fabrication.

4b. Role of ions on the conductance of the solution and E-Chem grafting

To investigate the impact of different counter ions on the conductance of the solution and E-Chem grafting of benzimidazole on ITO, we have performed solution phase electrochemical impedance spectroscopy measurements and E-Chem grafting by utilizing three different electrolytes to provide different counter ions. For this purpose, 0.1 M tetrabutylammonium tetrafluoroborate, tetrabutylammonium hexafluorophosphate, and tetrabutylammonium perchlorate in acetonitrile were used as an electrolyte. All the experimental conditions except different electrolytes were kept identical during these measurements.

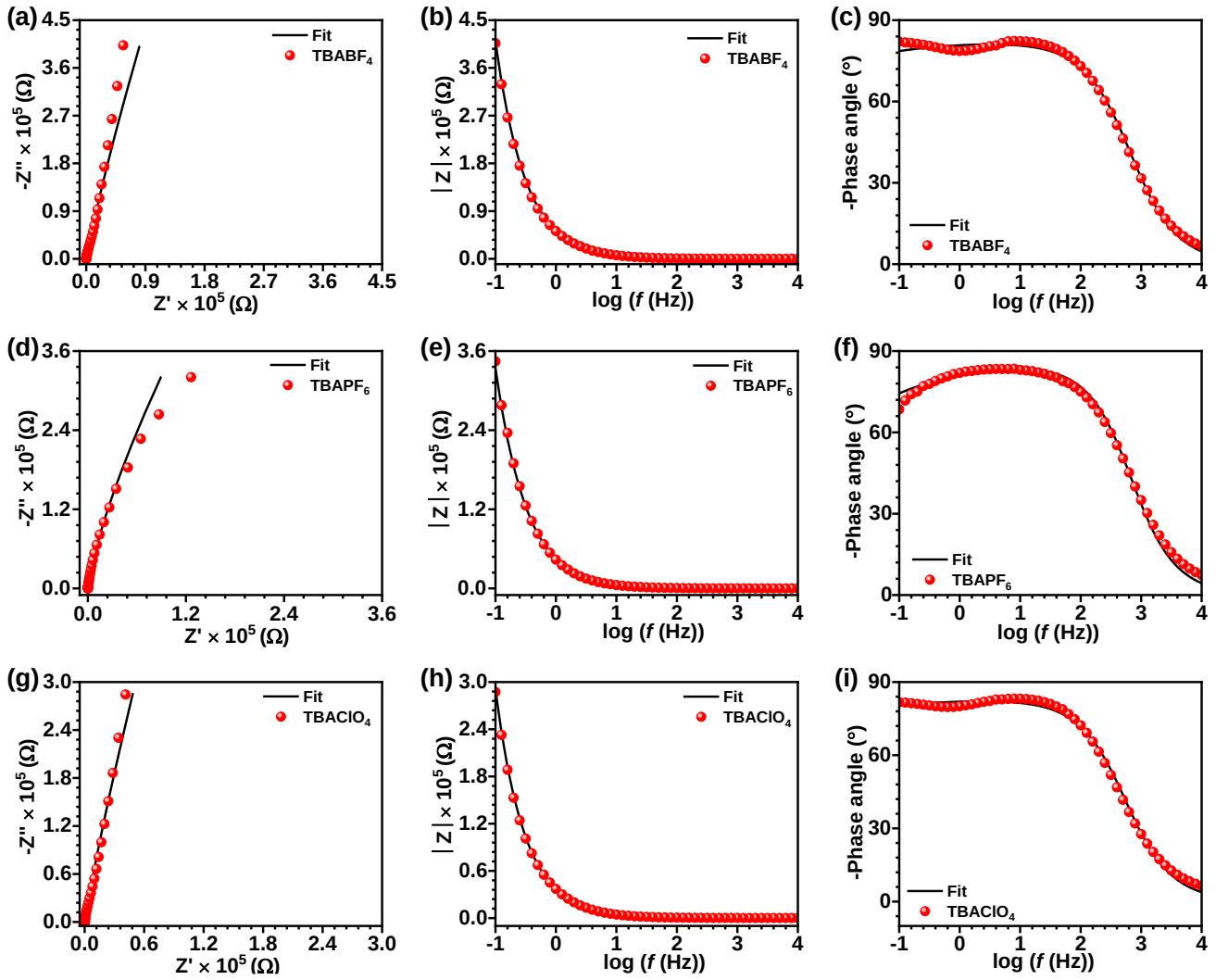

Figure S6. Nyquist and Bode plots at V= 0 DC voltage in the frequency range 10^4 to 0.1 Hz with 10 mV of AC amplitude for 0.1 M (a-c) tetrabutylammonium fluoroborate, (d-f) tetrabutylammonium hexafluorophosphate, and (g-i) tetrabutylammonium perchlorate electrolytes in acetonitrile employing ITO as a working electrode, $Ag/AgNO_3$ as reference and Pt wire as counter electrodes respectively.

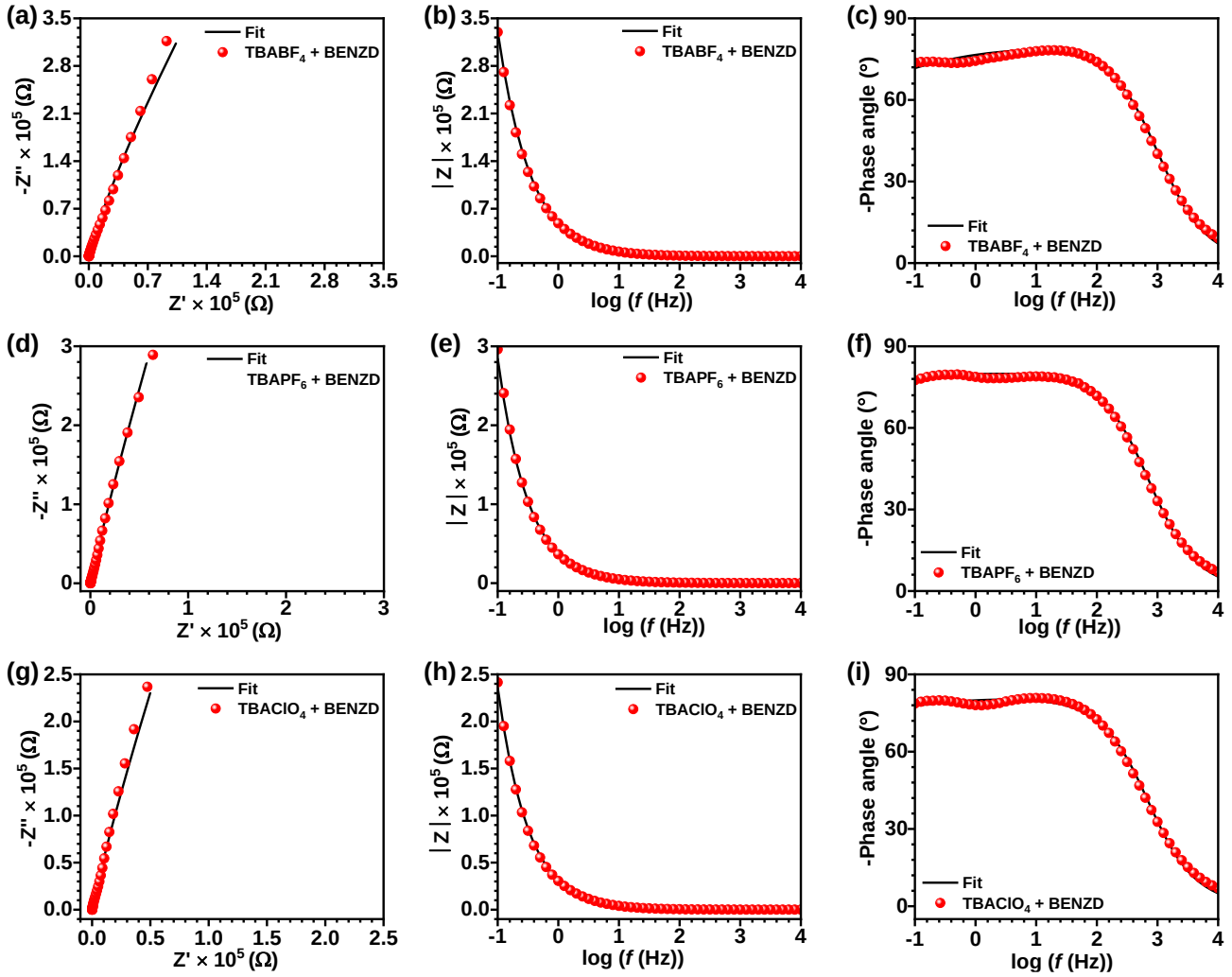

Figure S7. Nyquist and Bode plots at V= 0 DC voltage in the frequency range 10^4 to 0.1 Hz with 10 mV of AC amplitude for mixture of 2 mM benzimidazole diazonium and 0.1 M (a-c) tetrabutylammonium fluoroborate, (d-f) tetrabutylammonium hexafluorophosphate, and (g-i) tetrabutylammonium perchlorate electrolytes in acetonitrile employing ITO as a working electrode, $Ag/AgNO_3$ as reference and Pt wire as counter electrodes respectively.

Table S2: Value of Fitting parameters obtained from solution phase EIS data with varying electrolytes having different counterions and BENZD at 10 mV of AC perturbation in 10^4 Hz to 0.1 Hz frequency range.

Element	R_s (Ω)	W (μMho*S^1/2)	CPE		G (Ω^{-1})
			Yo (μMho*S^N)	N	From series resistance R_s
$TBABF_4$	141	0.342	3.42	0.916	7.09×10^{-3}
$TBABF_4$ + BENZD	105	1.04	3.52	0.9	9.52×10^{-3}
$TBAPF_6$	93.1	1.18	3.49	0.959	10.74×10^{-3}
$TBAPF_6$ + BENZD	102	0.344	4.99	0.9	9.80×10^{-3}
$TBAClO_4$	108	0.355	4.59	0.925	9.25×10^{-3}
$TBAClO_4$ + BENZD	84.1	0.605	5.86	0.907	11.89×10^{-3}

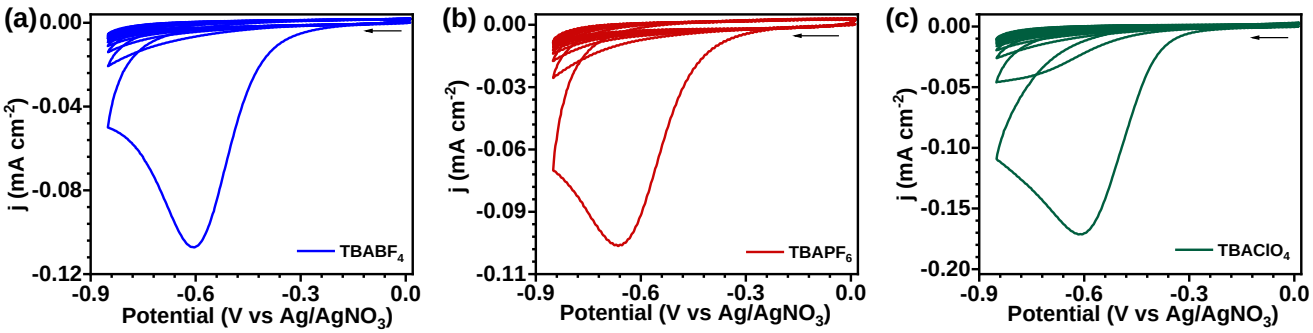

Figure S8. Cyclic voltammogram of electrochemically grafted BENZ molecular layers on commercial ITO electrodes utilizing 2 mM BENZD and 0.1 M of different electrolytes (a) tetrabutylammonium tetrafluoroborate, (b) tetrabutylammonium hexafluorophosphate, and (c) tetrabutylammonium perchlorate in acetonitrile. $Ag/AgNO_3$ and Pt wire were utilized as reference and counter electrodes respectively.

Table S3. Surface coverage of benzimidazole-based thin film on ITO utilizing different electrolytes during E-Chem grafting.

S.N.	Electrolyte	CV cycles	Potential window (V)	Observed diazonium reduction potential	Surface Coverage (mol cm^{-2})
1.	$TBABF_4$	12	0.01-(-0.85)	-0.605 V	3.74×10^{-9}
2.	$TBAPF_6$	12	0.01-(-0.85)	-0.663 V	3.78×10^{-9}
3.	$TBAClO_4$	12	0.01-(-0.85)	-0.607 V	7.5×10^{-9}

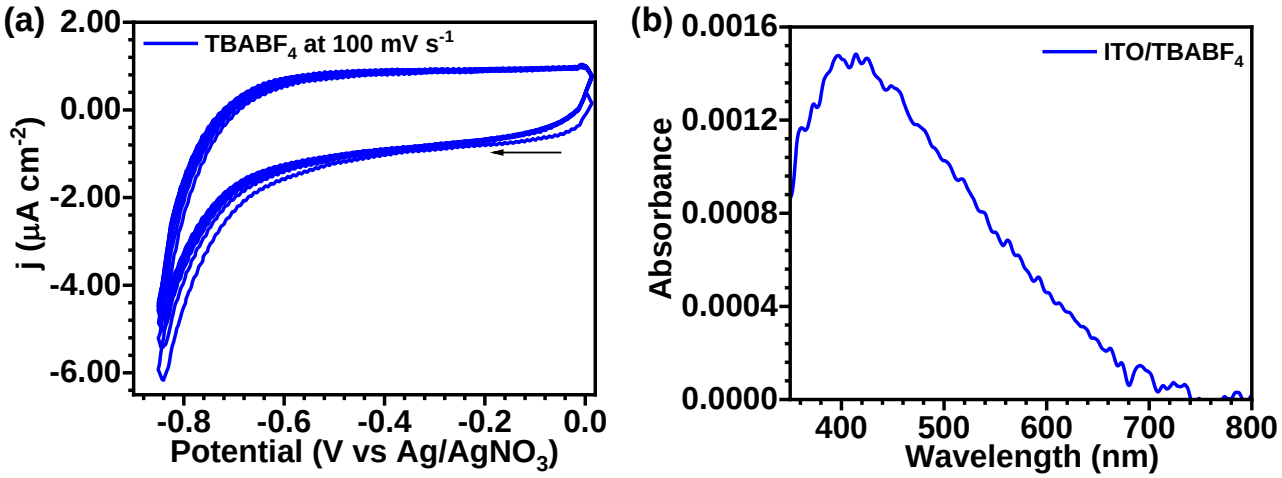

Figure S9. (a) Cyclic voltammogram of 0.1 M of tetrabutylammonium tetrafluoroborate in 0.01 V to -0.85 V potential window employing 12 scans at 100 mV s^{-1} on commercial ITO electrodes displayed no characteristic reduction peak of tetrabutyl ammonium salt. $Ag/AgNO_3$ and Pt wire were utilized as reference and counter electrodes respectively, (b) UV-Vis spectrum for the ITO used for CV in (a) shows an absorption band at 412 nm.

5. AFM measurements

The thickness of Film-1, Film-2, and Film-3 was calculated by AFM measurements. To make a glass/BENZ interface, 1 mm × 1 mm ITO films at the center of 2.5 cm × 1 cm ITO electrodes were etched out by applying conc. HCl and Zn dust powder for 10 seconds. After E-Chem grafting the total height (ITO+BENZ Films) at the interface was calculated for all samples. The actual height of the BENZ layer was calculated by subtracting the ITO height (calculated by AFM on bare ITO **Figure S10**) from the total sample height (ITO+BENZ Films, **Figure S11,** and **Table S1**).

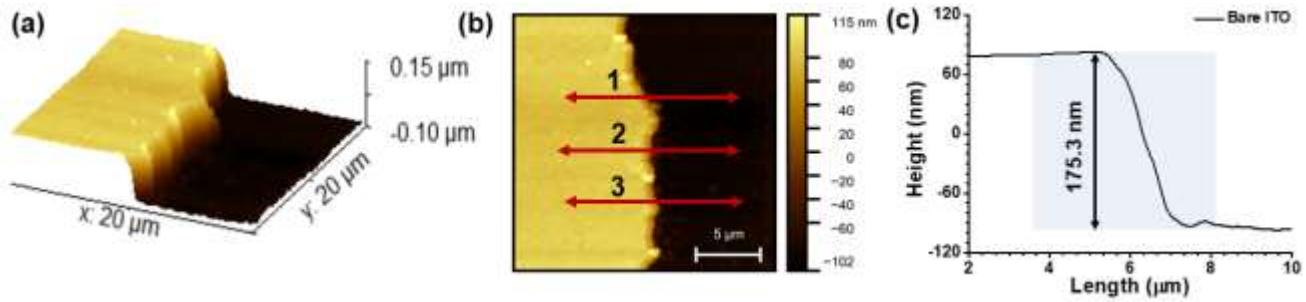

Figure S10. (a) 3-D, (b) 2-D AFM image of ITO/glass interface, and (c) line profile ITO/glass interface.

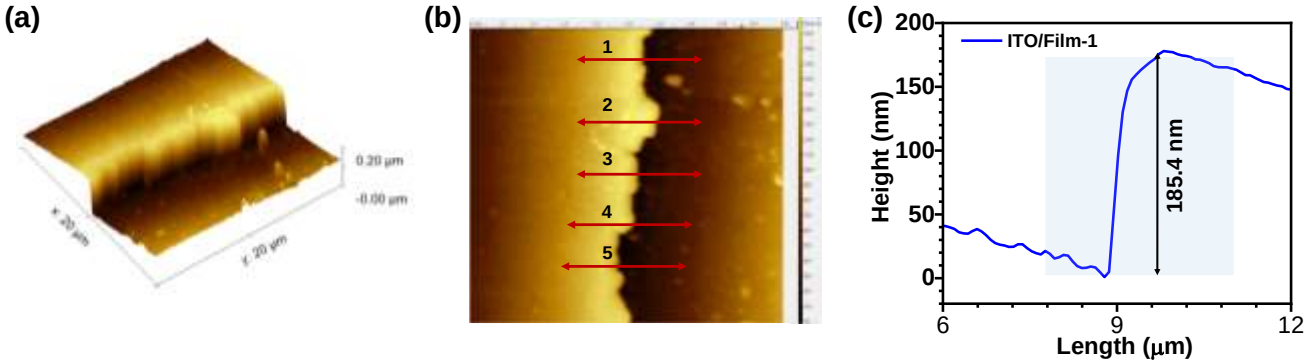

Figure S11. (a) 3-D and (b) 2-D AFM image of glass/ITO-BENZ interface and (c) line profile glass/ ITO-BENZ interface in Film-1

6. Calculation of the approximate number of BENZ layers in E-Chem grafted Film-1, Film-2, and Film-3

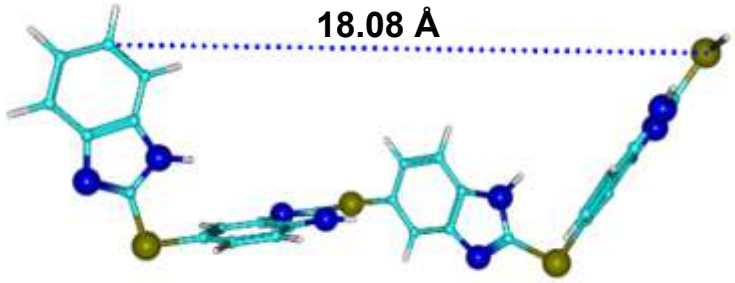

Figure S12. Optimized structure of 4 units of benzimidazole linked by C-S-C linkage with the length of the molecule measured between the carbon (that forms a bond with the bottom ITO electrode in grafted BENZ layers) of the aromatic ring at one end and sulfur atom at the other end of the molecule.

Table S4. The approximate number of BENZ units in electrochemically grown Film-1, Film-2, and Film-3 on ITO (calculated as per Figure S12).

	Film-1	*Film-2*	*Film-3*
No. of approximate BENZ molecular layers	22	32	41

7. Static water contact angle measurements

Before static water contact angle measurements the ITO substrate was cleaned as described in section S1 (for bare ITO). ITO substrate was modified with BENZ layers of different thicknesses employing the electrochemical grafting method as mentioned in section S4.

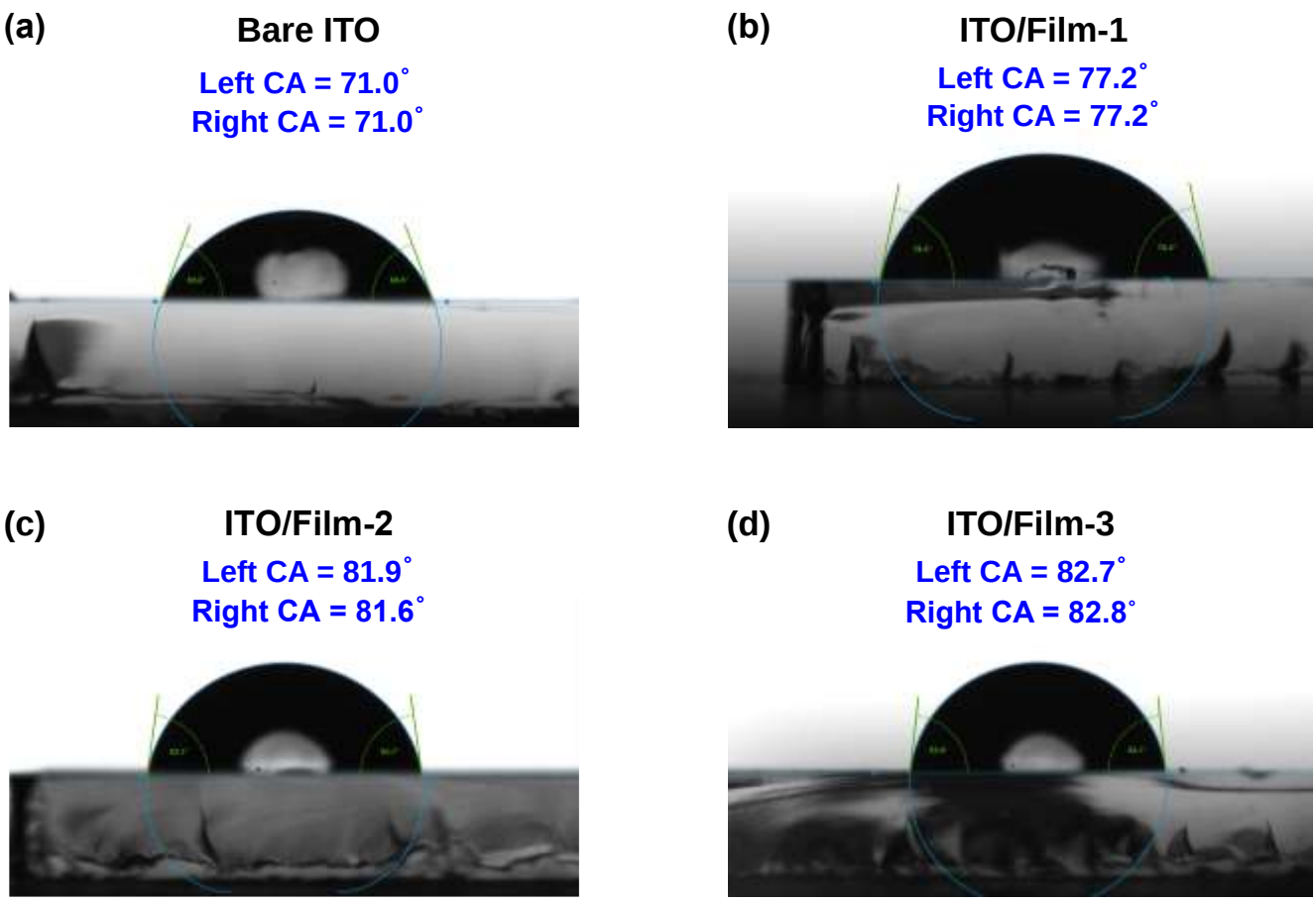

Figure S13. Static water contact angle measurements before and after modification of ITO substrate with BENZ layers of different thicknesses (a) bare ITO, (b) ITO/Film-1, (c) ITO/Film-2, and (d) ITO/Film-3.

Table S5: The average value of static water contact angle for bare ITO, ITO/Film-1, ITO/Film-2, and ITO/Film-3

Sample	CA left (deg)			Average CA left (deg)	CA right (deg)			Average CA right (deg)
Bare ITO	69.6	69.6	73.8	71 ± 2.42	69.6	69.6	73.8	71 ± 2.42
ITO/Film-1	76	78.4	77.2	77.2 ± 1.2	76	78.4	77.2	77.2 ± 1.2
ITO/Film-2	83	82.1	80.8	81.96 ± 1.10	83	82.1	79.9	81.6 ± 1.59
ITO/Film-3	82.8	83.6	81.8	82.73 ± 0.90	82.3	84.1	82.1	82.83 ± 1.10

8. Thin film XRD

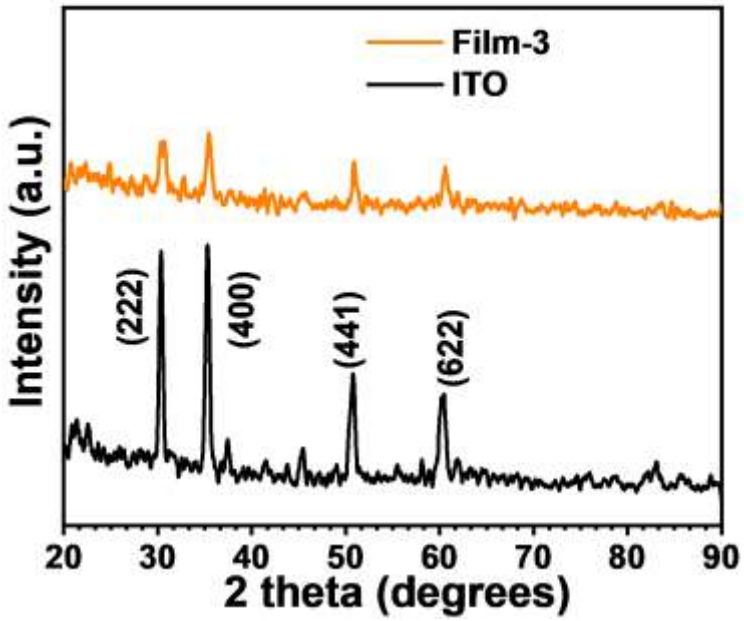

Figure S14. XRD patterns of bare ITO and Film-3.

9a. UV-vis spectra of Films 1-3

The UV-vis spectra of BENZ molecular layers on ITO show an absorption peak at 391 nm (**Figure S15(a)**). The absorbance at 391 nm increased continuously with an increase in the number of CV scans for E-Chem grafting of Film-1 to Film-3 (**Figure S15(b)**).

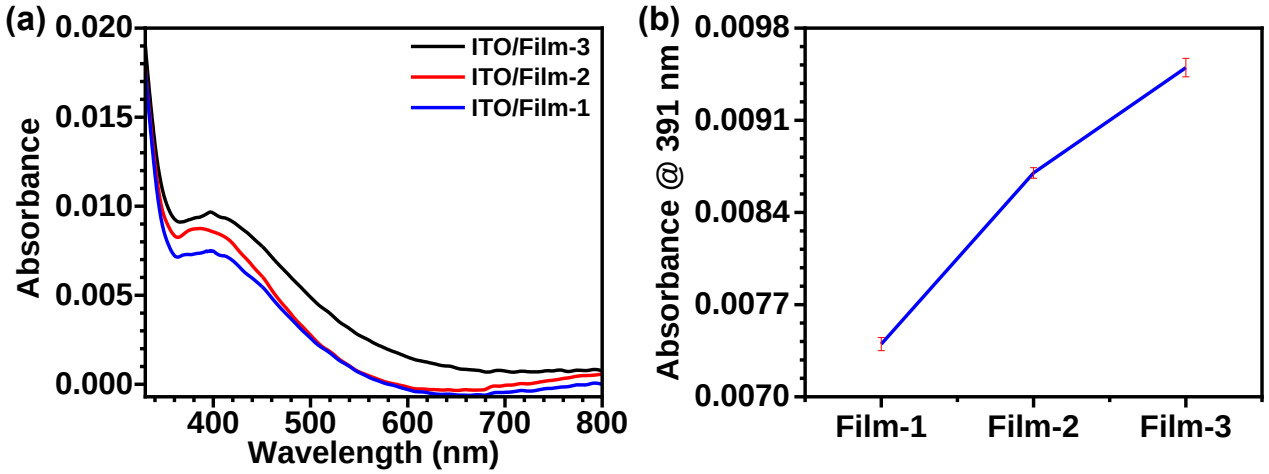

Figure S15. (a) Comparison of UV-vis spectra of Film 1-3 and, and (b) Absorbance of Film 1-3 at 391 nm.

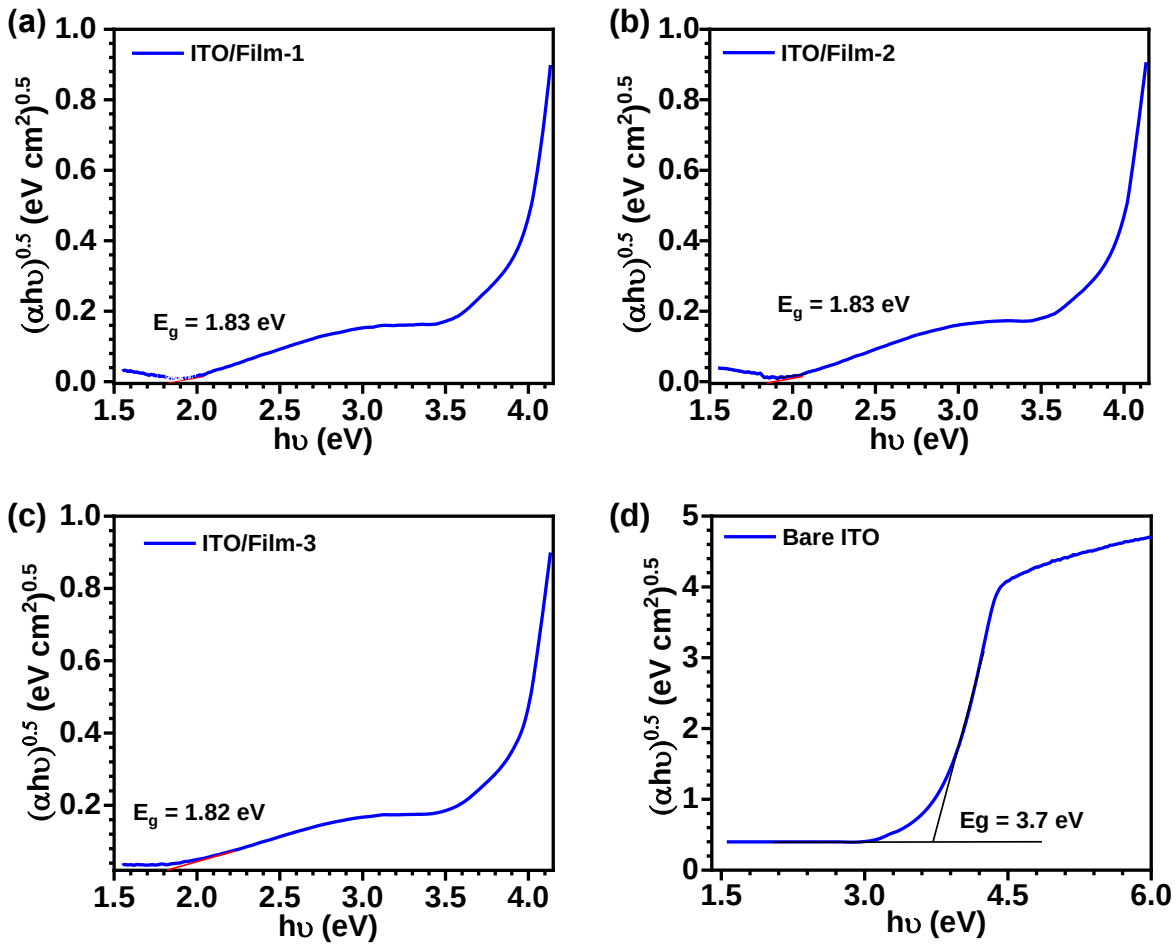

Figure S16. Tauc plot for direct band gap calculation from experimental thin film UV-visible data (a) Film-1 (b) Film-2, (c) Film-3, and (d) bare ITO.

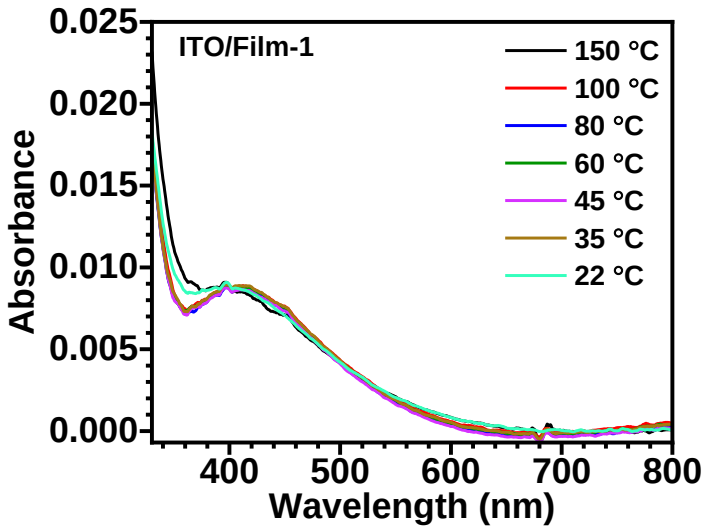

Figure S17. Temperature-dependent UV-vis spectra for ITO/Film-1 demonstrating the thermal stability of BENZ thin film up to 150 ˚C.

9b. Thin film FTIR and Raman spectrum of ITO/Film-3

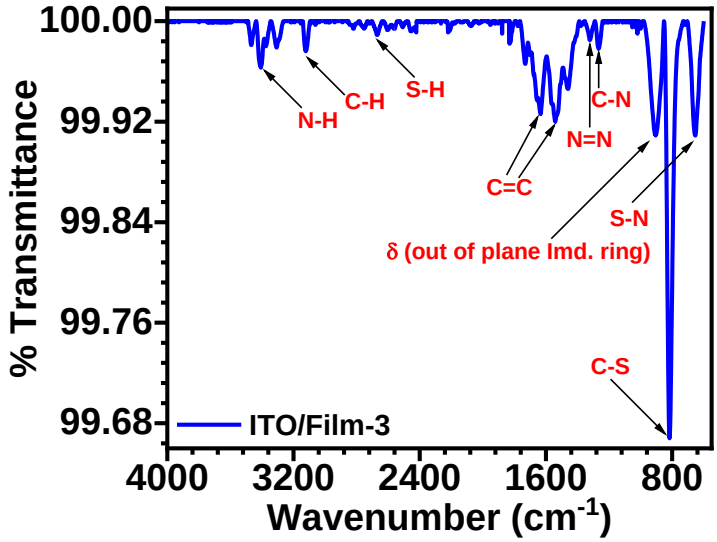

Figure S18. Thin film characterization of benzimidazole-modified ITO employing (a) ATR-FTIR, bare ITO taken as background. The FTIR spectrum showcased the characteristic peaks of the benzimidazole molecular thin film.

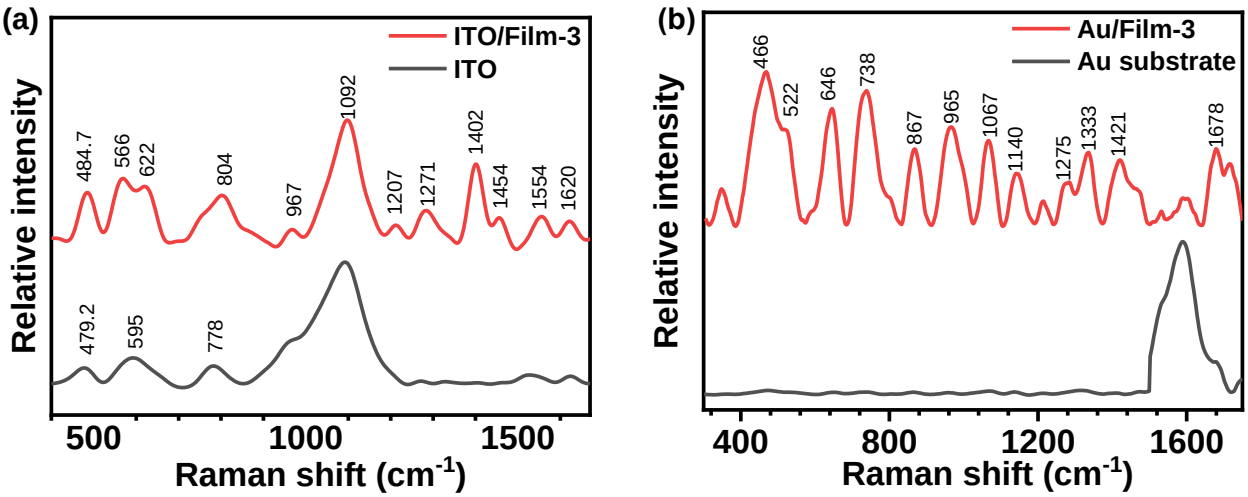

Figure S19. Thin film characterization of E-Chem grafted BENZ layers using Raman spectroscopy. (a) Raman spectra for ITO/Film-3, and bare ITO, (b) Raman spectra for Au/Film-3 and Au substrate.

Table S6: Assignment of Raman peaks observed for ITO/BENZ and Au/BENZ thin films according to the literature reports.[4–6]

ITO/Film-3	Au/Film-3	Bond vibration assignments
566	522	τ(N-H)
622	646	ν(C-S)
	738	τ(C-H)
804	867	ν(N-H)
967	965	ν(S-H)
	1067	ν(S-N)
	1140	δ(N-H)
1271	1275	ν(C-H)
	1333	δ(C-H)
1402	1421	β(C-N)
1454	1471	ν(N-C) + ν(C-C)
1554	1591	ν(C-C) + ν(N=N)
1620	1678	ν(C-C)

ν is stretching vibration, δ, β in-plane bending and τ is out-of-plane bending modes of vibration.

10. XPS measurements

High-resolution spectra for bare ITO in regions of C1s, N1s, O1s, S2p, In3d, and Sn3d are shown in **Figure S20,** and corresponding binding energies are summarized in **Table S7**.

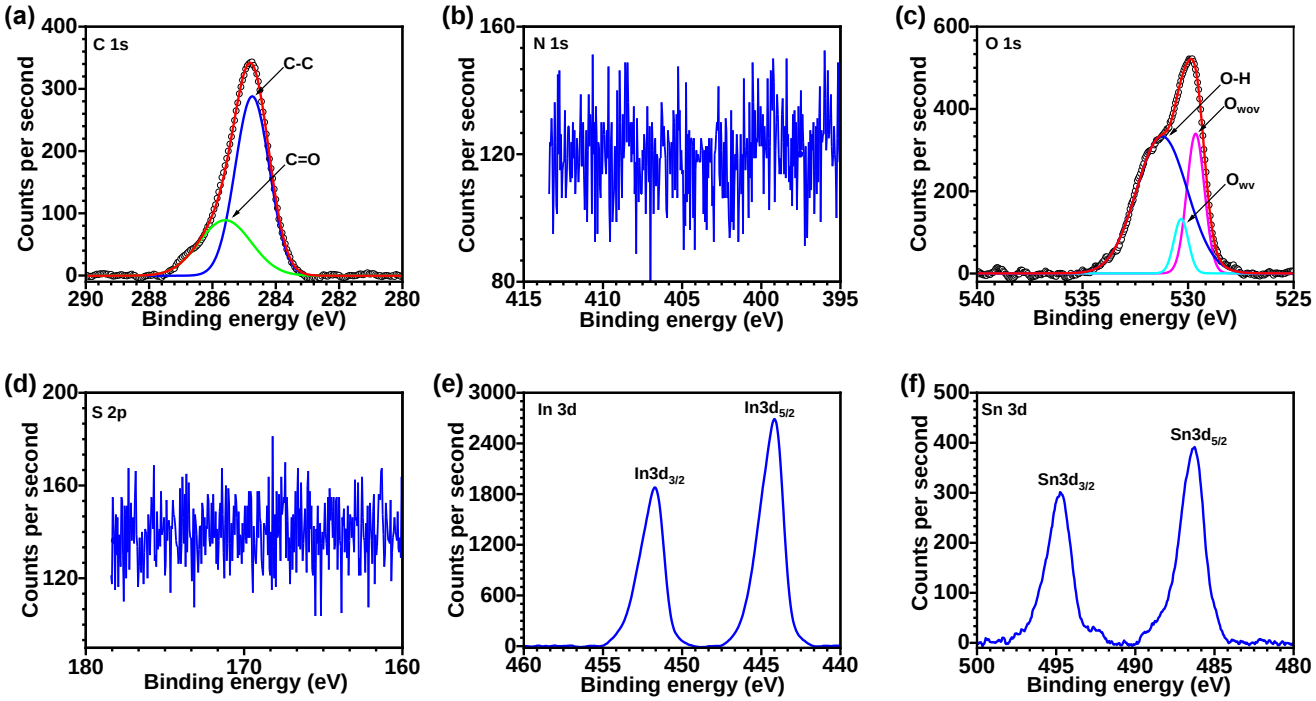

Figure S20. High resolution and deconvoluted XPS spectra of (a) C1s, (b) N1s (c) O1s, (d) S2p, (e) In3d, and (f) Sn3d of bare ITO.

Table S7. XPS analysis of bare ITO and Film-1.

S.N.	Material	Element	State/Term	Binding energy (eV)
1.	Bare ITO	C	1s	284.74 ± 0.009 285.59 ± 0.009
		N	1s	-
		O	1s	529.64 ± 0.01 530.32 ± 0.017 531.23 ± 0.1
		S	2p	-
		In	3d5/2 3d3/2	444.18 ± 0.01 451.70 ± 0.01
		Sn	3d5/2 3d3/2	486.29 ± 0.01 494.77 ± 0.01
		C	1s	284.2 ± 0.009 284.8 ± 0.009 285.43 ± 0.009 285.7 ± 0.007

				286.17 ± 0.008
				287 ± 0.005
2.	Film-1	N	1s	398.65 ± 0.02
				400.40 ± 0.03
				402.24 ± 0.23
		O	1s	529.78 ± 0.29
				530.36 ± 0.11
				531.14 ± 0.13
				532.09 ± 0.19
		S	2p3/2	163.76 ± 0.06
			2p1/2	164.84 ± 0.09
			2p3/2	168.54 ± 0.07
			2p1/2	169.66 ± 0.07
		In	3d5/2	444.94 ± 0.009
			3d3/2	452.48 ± 0.01
		Sn	3d5/2	486.91 ± 0.01
			3d3/2	495.29 ± 0.01

11. Al top electrode deposition

After successful electrochemical grafting of molecular layers, a shadow mask with six parallel lines of 500 µm width openings was placed in a crossbar fashion i.e., perpendicular to the bottom ITO. Chips and sample holder were transferred to a thermal evaporator (Hind High Vac HVV BC 300) and pumped down for 3 h to make chamber pressure 5 $\times 10^{-6}$ mbar. The top contacts were made with 50 nm of evaporated Aluminium (Al). ITO/BENZ/Al produced an active junction area of 0.0025 cm^2 (**Figure S21**).

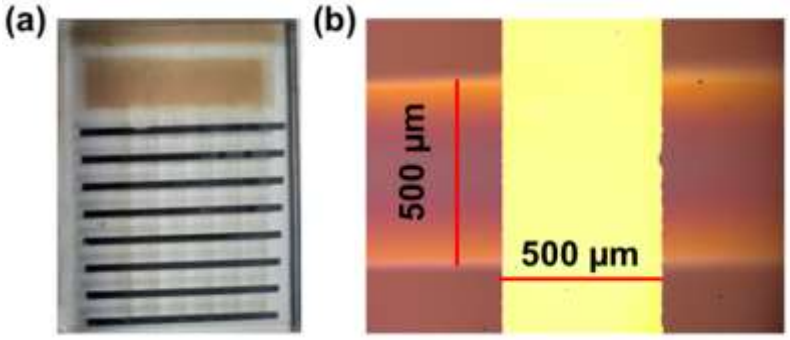

Figure S21. (a) Digital image of fabricated molecular junctions and (b) optical image of a molecular junction.

12. *I-V* measurements and calculation of parallel plate capacitance in molecular junctions

The ITO/Al junction shows almost Ohmic behavior also no *j-V* hysteresis was observed in the ITO/Al junction (**Figure S23**). *j-V* hysteresis of molecular junctions (ITO/Film-1/Al, ITO/Film-2/Al, and ITO/Film-3/Al MJs) were obtained in the range of +1.5 V to -1 V at a scan rate of 10 mV s^{-1} to 1000 mV s^{-1} (**Figure S29**). The capacitance in molecular junctions was determined using equation (2);

$$C = \frac{\int I dv}{v \times A \times \Delta E} \quad (2)$$

Where I is the current (in ampere), C is the parallel plate capacitance (F cm^{-2}), ν is the scan rate (V s^{-1}) of the I-V cycle and A is the area of junction (in cm^{-2}). The ITO/Film-1/Al MJs were very stable up to over 1200 continuous *j-V* hysteresis loops even at a higher scan rate of 500 mV s^{-1} and retained 95% of initial capacitance (**Figure S30**).

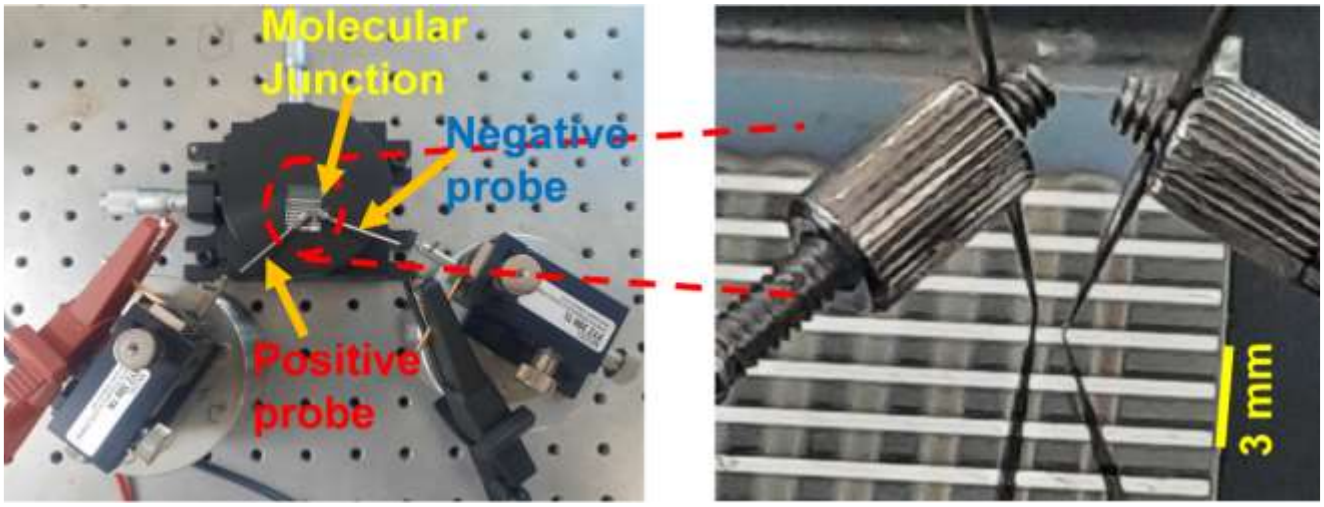

Figure S22. (a) Two-probe *I-V* measurement set-up with ITO contacted to the negative probe and Al to the positive probe, and (b) zoomed view showing the crossbar MJs contacted to two probes while performing DC-based electrical measurements.

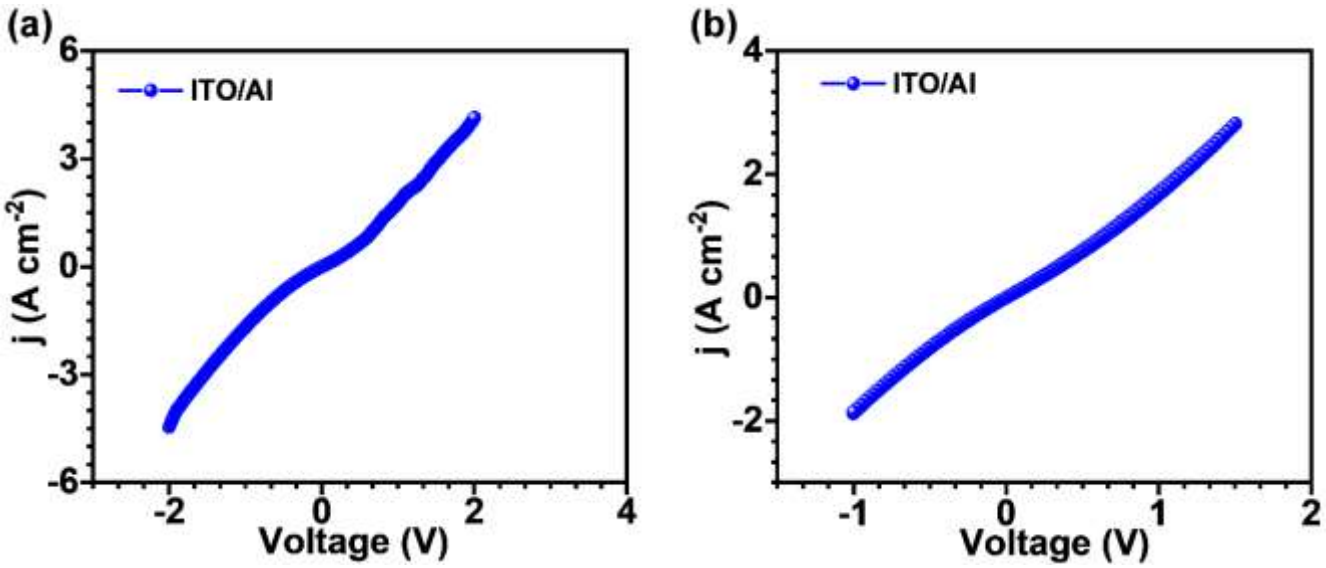

Figure S23. (a) *j-V* curve of ITO-Al junction and (b)) *j-V* loop curve showing no hysteresis for ITO-Al junction.

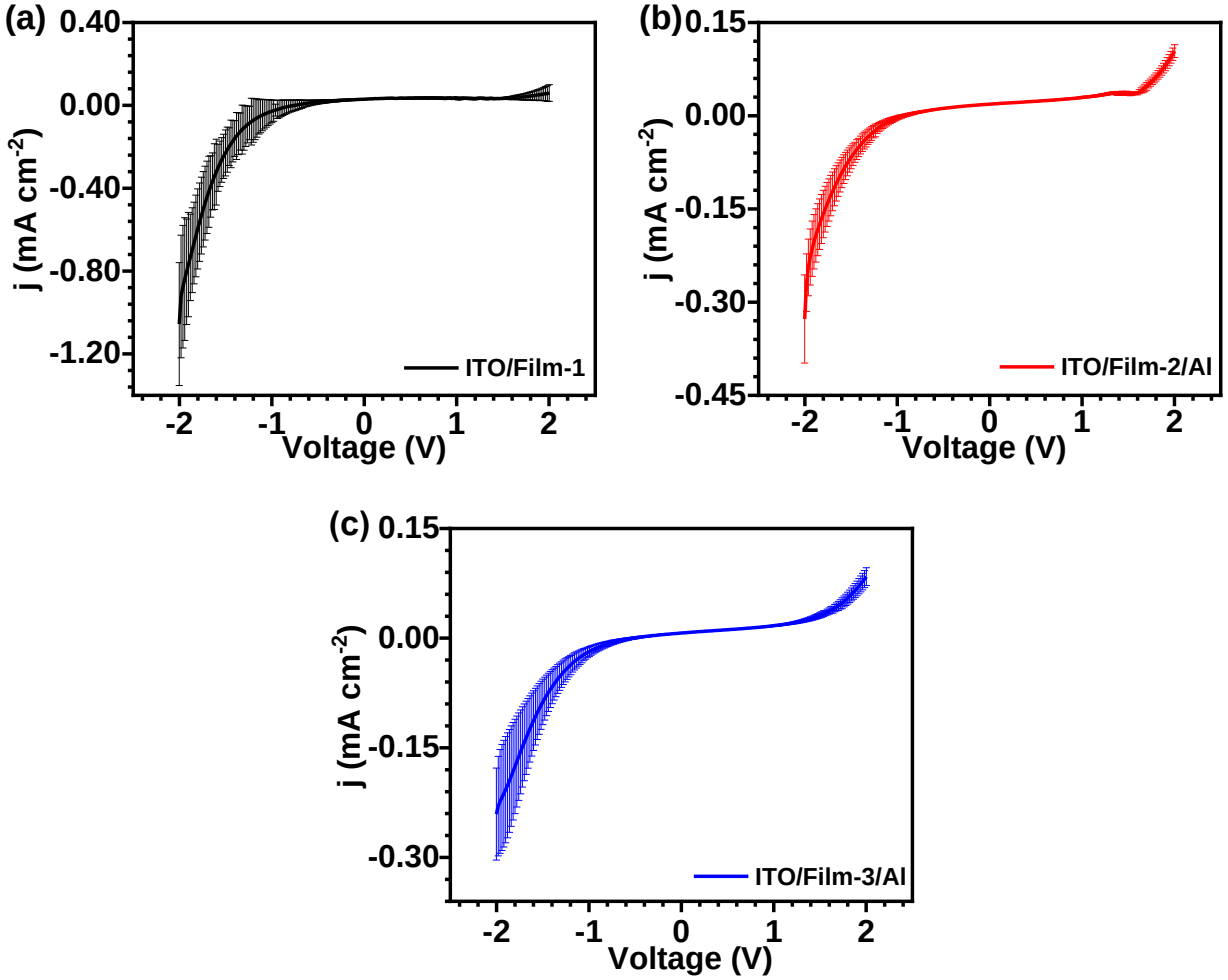

Figure S24. Average *j-V* curves in ±2 V window with standard deviation for (a) ITO/Film-1/Al, (b) ITO/Film-2/Al, and (c) ITO/Film-3/Al MJs.

12.a. Experimental investigation of charge conduction in ITO/BENZ/Al MJs

Hall measurements

To investigate the type of charge carriers, mobility, and nature of charge transport, the Hall effect was studied on BENZ molecular layers grafted on a commercial ITO electrode. The silver paste was used to make four probe contacts. The bare ITO electrode was taken as a reference sample. The external magnetic field of 0.5 T was applied.

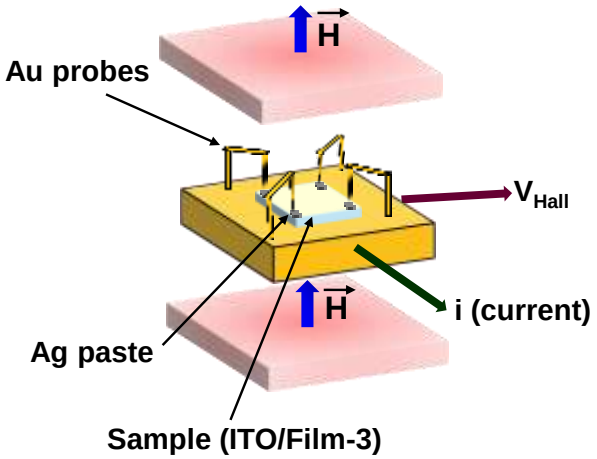

Figure S25. Schematic representation of the Hall measurements set up employed for ITO/Film-3. Silver (Ag) paste was used to make four contacts for Hall measurements.

Table S8. Hall measurement parameters for bare ITO and ITO/Film-3.

Parameters	ITO	ITO/Film-3
Bulk concentration (cm^{-3})	-2.29×10^{21}	-3.61×10^{18}
Sheet concentration (cm^{-2})	-2.29×10^{16}	-1.80×10^{14}
Sheet resistance ($\Omega\ sq^{-1}$)	11.3	5.18×10^{5}
Resistivity(Ω cm)	1.17×10^{-4}	25.9
Mobility ($cm^2\ V\ s^{-1}$)	23.4	0.66
Average Hall coefficient ($cm^3\ C^{-1}$)	-2.73×10^{-3}	-1.72

Mott-Schottky analysis

Mott-Schottky analysis for bare ITO and ITO/Film-3 was performed to analyze the nature of the material (p or n-type) and calculate the flat-band potential from the x-intercept of the reciprocal of the capacitance square versus the V_{dc} plot using Mott-Schottky equation (i) and (ii)[7]

$$\frac{1}{C_{sc}^2} = \frac{2(\frac{\Delta\varphi RT}{F})}{f\varepsilon_0\varepsilon N_{SC}} \quad \text{.....(i)}$$

$$\Delta\varphi = V - V_{fb} \text{ .....(ii)}$$

C_{sc} is space charge capacity, $\Delta\varphi = V - V_{fb}$ is the voltage drop in the space-charge layer, R is the gas constant, F is the Faraday constant, ε the dielectric constant of the semiconductor, ε_0 the permittivity of vacuum and N_{SC} is the ionized donor dopant concentration, V_{fb} represents the flat band potential. Flat band potential is of utmost importance for the determination of the valence and conduction band edge of the material.

The DC potential was varied with a 0.1 V gap from -1 to +1 V, and EIS was recorded at different frequencies while the AC voltage was fixed at 10 mV. The mott-Schottky measurements were done by using Gamry 600+ Reference Potentiostat. We have analyzed Mott-Schottky plots at 5 kHz. 1.5 kHz, 1 kHz, and 0.5 kHz. Although Mott-Schottky's theory suggests that plots should be independent of the measuring frequency this behavior is rarely observed for semiconductor electrodes which is attributed to the surface roughness, dielectric relaxation, and the influence of surface states.[8] The flat-band potential with reference to vacuum is calculated using the equation given below.[7]

$$V_{Vacuum} = [(-V_{NHE}) - 4.5] \text{..... (iii)}$$

The potential of the $Ag/AgNO_3$ reference electrode in acetonitrile solvent with respect to NHE (Normal Hydrogen electrode) is +0.54 V which is utilized for the conversion of flat-band potential value with respect to NHE .[8]

Reciprocal of the capacitance square versus the V_{dc} plots for ITO and ITO/Film-3 exhibit a positive slope that signfies the n-type nature of ITO and ITO/Film-3. The flat-band potential (V_{fb}) is used for calculating the conduction band minima (E_{CB}) for n-type ITO and ITO/Film-3 using the equation given below[8]

$$E_{CB} = V_{fb} + kT\, ln\frac{N_{SC}}{N_{CB}} \quad \text{.....(iv)}$$

Where k is Boltzmann constant (eV K^{-1}), T is the temperature (K), N_{SC} and N_{CB} are the effective density of states in space charge region calculated from the slope of reciprocal of the capacitance square versus the V_{dc} plots (M-S plot) and effective density of states in the conduction band of the n-type semiconductor.

N_{CB} is approximated by using the relation

$$N_{CB} = 2\left(\frac{2\Pi m_e^* k_B T}{h^2}\right)^{3/2} \text{.....(v)}$$

Where k_B is Boltzmann constant (m^2 Kgs^{-2} K^{-1}), T is the temperature (K), m_e^* is the effective mass of the electron (0.3 times of m_e taken for ITO), h is Planck's constant (m^2 Kg s^{-1}).

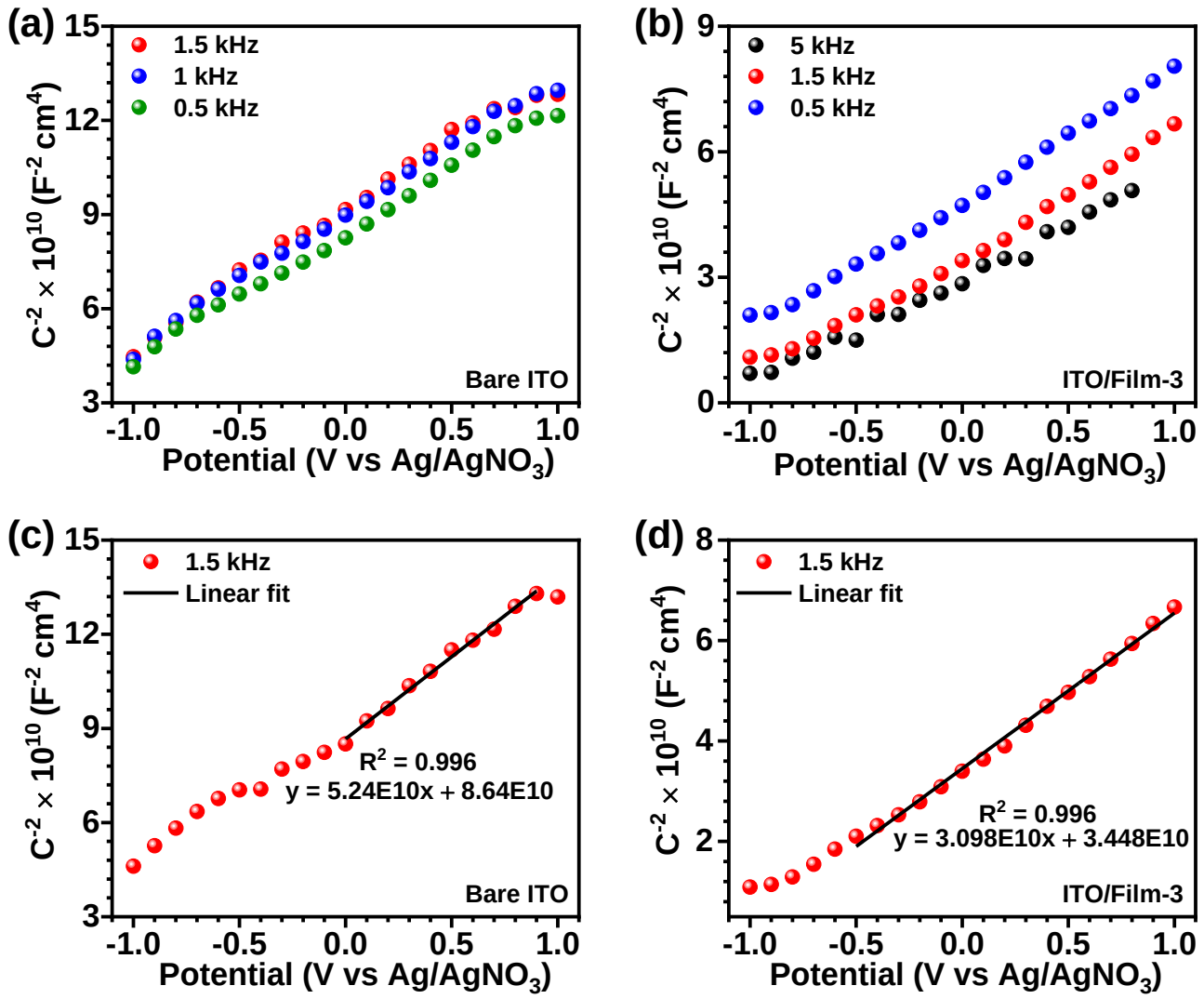

Figure S26. Mott-Schottky (M-S) analysis of Bare ITO and ITO/Film-3 by utilizing bare ITO and ITO/Film-3 as working electrode, $Ag/AgNO_3$ as reference, and Pt wire as counter electrode in 0.1 M $TBABF_4$ electrolyte in acetonitrile solvent. The plot of the reciprocal of the capacitance square versus the V_{dc} (measured with reference to $Ag/AgNO_3$ reference electrode) in ±1 V DC voltage range with 0.1 V gap at different frequencies (a) For bare ITO, (b) for ITO/Film-3, demonstration of linear fitting of M-S plot for calculation of flatband potential (c) for bare ITO, and (d) for ITO/Film-3.

Table S9. Calculation of valence band maxima (VBM) and conduction band minima (CBM) using flat-band potential (V_{fb}) from M-S measurements, and optical band gap for bare ITO.

	V_{fb} vs Ag/Ag^+ (V)	V_{fb} vs NHE (V)	$V_{fb\ (vacuum)}$ (eV)	E_{VBM} (eV)	E_{CBM} (eV)
1.5 kHz	**-1.65**	**-1.11**	**-3.39**	**-7.06**	**-3.36**
1 kHz	**-1.83**	**-1.29**	**-3.21**	**-6.92**	**-3.22**
0.5 kHz	**-1.57**	**-1.03**	**-3.47**	**-7.15**	**-3.45**

The optical band gap value used for bare ITO is 3.7 eV from thin film UV-vis data matches with the literature reports.[10]

Results for ITO show very little change in the flat band potential and conduction band minima and the effective mass of electron for benzimidazole molecule is not known, therefore, we have assumed the falt-band potential of ITO/Film-3 equal to conduction band minima.

Table S10. Calculation of valence band maxima (VBM) and conduction band minima (CBM) using flat-band potential (V_{fb}) from M-S measurements, and optical band gap (obtained from thin film UV-vis) for ITO/Film-3.

	V_{fb} vs Ag/Ag^+ (V)	V_{fb} vs NHE (V)	$V_{fb\ (vacuum)}$ (eV)	VBM_{vacuum} (eV)	CBM_{vacuum} (eV)
5 kHz	**-1.10**	**-0.56**	**-3.94**	**-5.76**	**-3.94**
1.5 kHz	**-0.8985**	**-0.3585**	**-4.14**	**-5.96**	**-4.14**
0.5 kHz	**-1.24**	**-0.70**	**-3.80**	**-5.62**	**-3.80**

Valence Band XPS spectra for Bare ITO and ITO/Film-3

The valence band edge (E_F-E_{VBM}) from the VBXPS spectrum for bare ITO and ITO/Film-3 was found to be 2.55 eV and 1.15 eV respectively. E_F is the Fermi energy level and E_{VBM} represents the valence band maxima. By taking E_F = -4.7 eV for ITO electrode, the valence band maxima for ITO lies at -7.25 eV (E_F- E_{VBM} = -4.7 eV – E_{VBM} = 2.55 eV, E_{VBM} = -4.7-2.55 = -7. 25 eV). The value of valence band maxima calculated from XPS is close to the value obtained from the Mott-Schottky analysis.

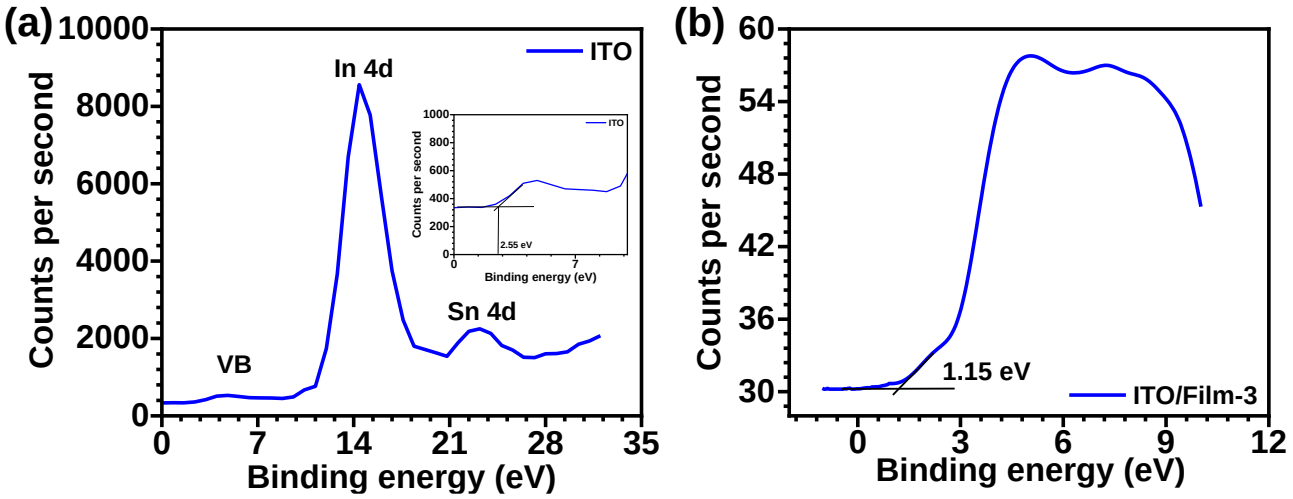

Figure S27. Low-binding energy region for Valence band XPS spectrum of (a) bare ITO, zoomed image showing valence band edge onset (E_F-E_{VBM}) at 2.55 eV, and (b) for ITO/Film-3 depicting valence band edge onset (E_F-E_{VBM}) at 1.15 eV.

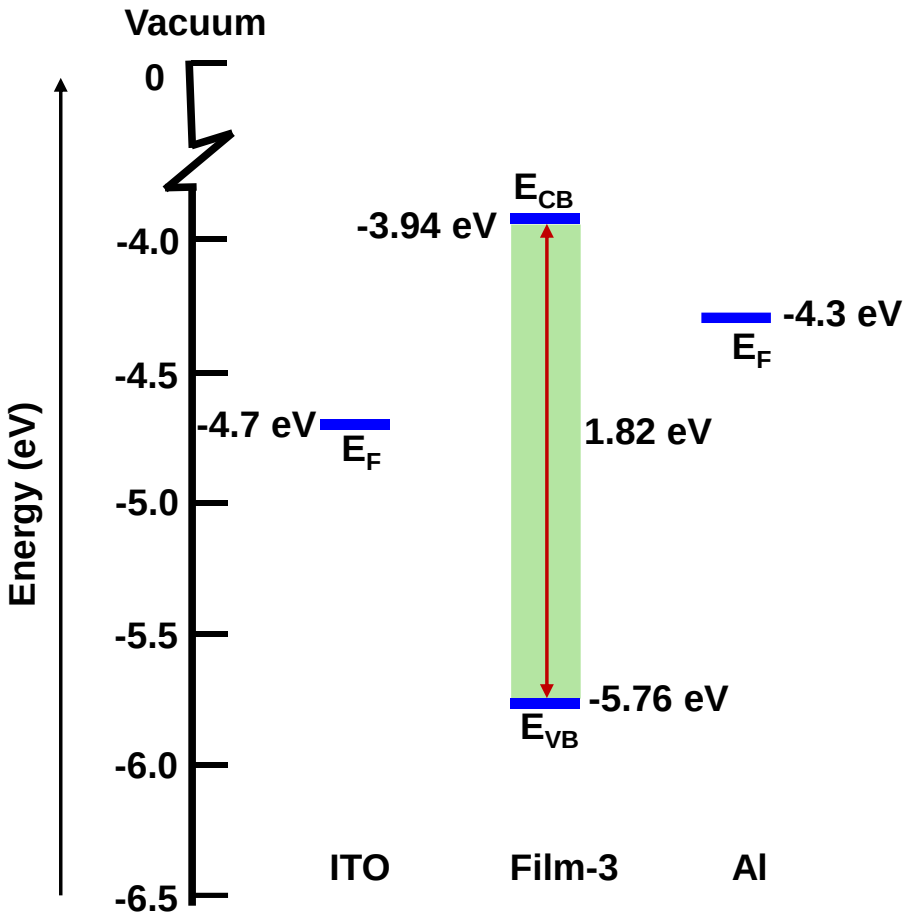

Figure S28. Energy profile diagram for the ITO/Film-3/Al MJs based on Mott-Schottky, VBXPS, thin-film UV-vis, and literature reports. E_F represents the Fermi energy level of the electrode, E_{VB} valence band maxima corresponds to the HOMO energy level, and E_{CB} conduction band minima corresponds to the LUMO level with reference to the vacuum level.

12.b. Scan rate-dependent charge storage analysis of ITO/BENZ/Al MJs

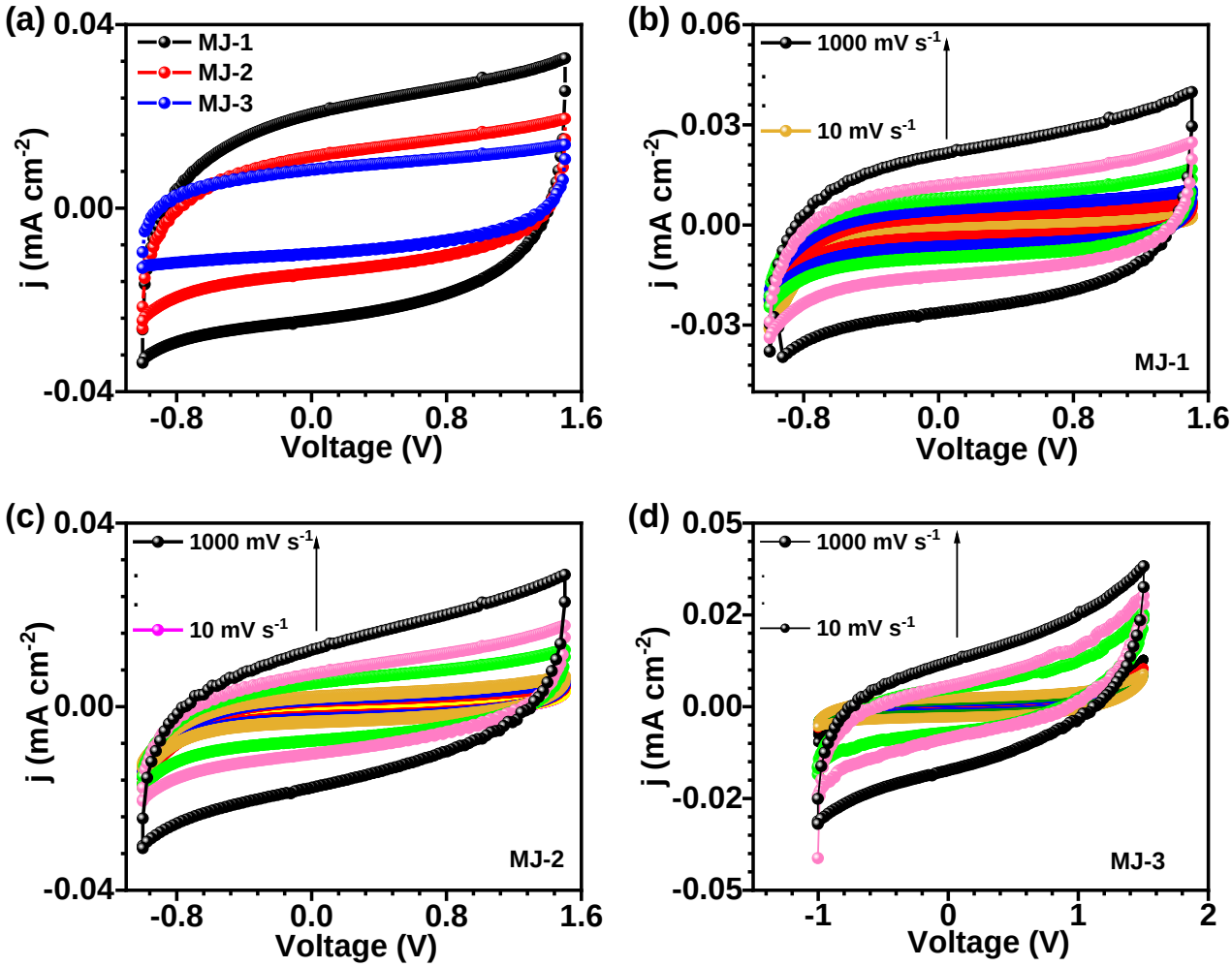

Figure S29. *j-V* hysteresis in ITO/BENZ/Al MJs (a) comparative hysteresis curve for ITO/Film-1/Al (MJ-1), ITO/Film-2/Al (MJ-2), and ITO/Film-3/Al (MJ-3) MJs at 500 mV s^{-1}, Scan rate-dependent *j-V* hysteresis in (b) ITO/Film-1/Al, (c) ITO/Film-2/Al, and (d) ITO/Film-3/Al MJs.

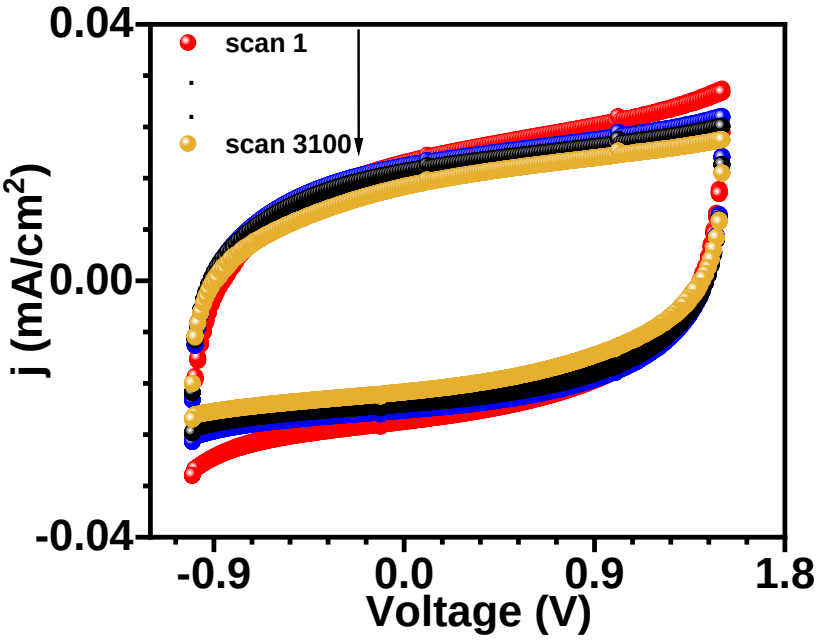

Figure S30. *j-V* hysteresis in ITO/Film-1/Al MJs up to 3100 loops.

13. Electrochemical impedance spectroscopy of molecular junction

Two probe electrical measurements were done in ITO/Al junction (reference device, **Figure S31**) and ITO/BENZ/Al junction. EIS measurements were done over a frequency region from 10^6 to 1 Hz with 100 mV AC amplitude. The obtained data were fitted with an equivalent Randle's circuit model, where R_u is uncompensated resistance (mainly contact resistance), R_{ct} is charge transfer resistance and CPE (Q) is a constant phase element.

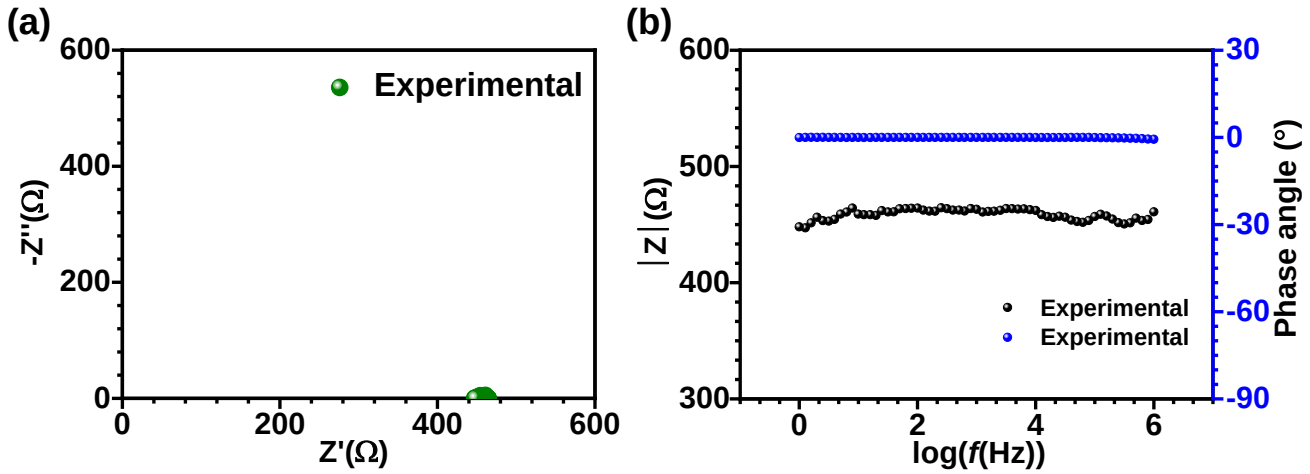

Figure S31. (a) Nyquist plot (b) Bode plot of ITO/Al junction at V= 0 DC voltage in the frequency range 10^6 to 1 Hz with 100 mV of AC amplitude.

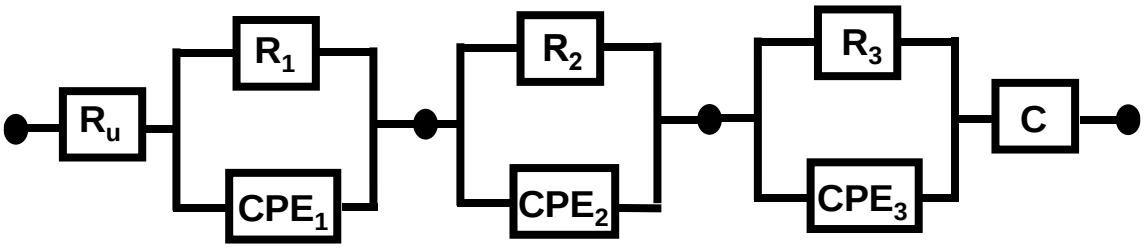

Figure S32. Circuit used for modeling of Electrochemical impedance spectroscopy data of ITO/Film-1/Al, ITO/Film-2/Al, and ITO/Film-3/Al MJs.

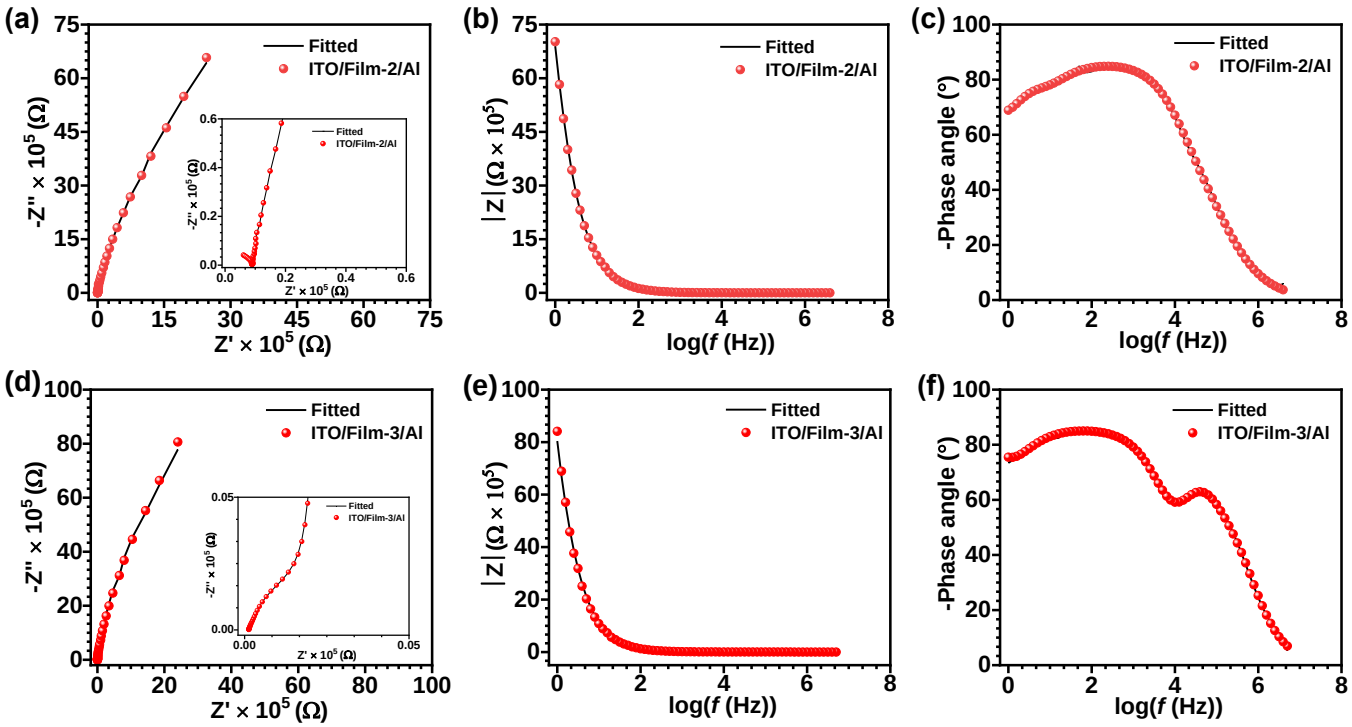

Figure S33. Nyquist and Bode plots at V= 0 DC voltage in the frequency range 10^6 to 1 Hz with 100 mV of AC amplitude for (a-c) ITO/Film-2/Al, and (d-f) ITO/Film-3/Al.

Table S11: value of Fitting parameters obtained from EIS data at 100 mV of AC perturbation for ITO/BENZ/Al junctions of different thicknesses.

Element	ITO/Film-1/Al	ITO/Film-2/Al	ITO/Film-3/Al
R_u (Ω)	284.2	279.3	125.6
R-1 (Ω)	874.1	416.8	3.478×10^{6}
Y_0-1 ($S^{*}s^{\wedge}a$)	21.31×10^{-9}	656.2×10^{-9}	44.81×10^{-9}
a-1	951.4×10^{-3}	672.5×10^{-3}	913.4×10^{-3}
R-2 (Ω)	6.181×10^{6}	4.928×10^{6}	96.11
Y_0-2 ($S^{*}s^{\wedge}a$)	50.15×10^{-9}	39.22×10^{-9}	48.28×10^{-9}
a-2	942.4×10^{-3}	945.1×10^{-3}	870.0×10^{-3}
R-3 (Ω)	274.8×10^{3}	234.2×10^{3}	1.412×10^{3}
Y_0-3 ($S^{*}s^{\wedge}a$)	90.51×10^{-9}	88.10×10^{-9}	11.94×10^{-9}
a-3	926.1×10^{-3}	932.6×10^{-3}	960.0×10^{-3}
C (F)	159.3×10^{-9}	38.33×10^{-9}	25.33×10^{-9}
Goodness of fit	3.11×10^{-3}	15.11×10^{-3}	500.6×10^{-6}

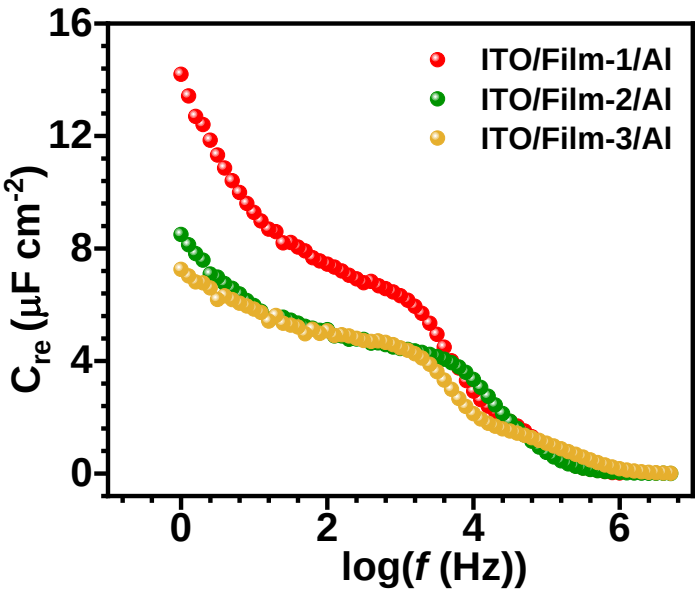

Figure S34. Frequency-dependent capacitive response of ITO/BENZ/Al MJs of varying thickness at V= 0 DC voltage in the frequency range 10^{6} to 1 Hz with 100 mV of AC amplitude.

14. Statistics data for MJs

Table S12: % yield of ITO/Film-1/Al, ITO/Film-2/Al, and ITO/Film-3/Al MJs

Sample	No. of junctions fabricated	No. of MJs in working condition	Yield (%)
ITO/Film-1/Al	40	26	65
ITO/Film-2/Al	40	24	60
ITO/Film-3/Al	40	28	70

15. Comparison of device performance to literature reports

Table S13: Comparison of ITO/BENZ/Al device performance to literature reports

Device configuration	Scan rate (mV s^{-1})	Areal capacitance	Reference
Ti/Cu/carbon-nanofibre/Al_2O_3	-	18.2 nF mm^{-2}	[11]
p-Si/Si-nanowires/HfO_2/Al	-	5.4 μF cm^{-2}	[12]
LightScribeGraphene micro supercapacitor	-	1.35 mF cm^{-2}	[13]
Si/carbon-nanofibre/Al_2O_3	-	15 nF mm^{-2}	[14]
Si-wafer/graphene oxide/Au	10	78.9 μF cm^{-2}	[15]
Si-wafer/Sulphur-doped-graphene/Au	10	~553 μF cm^{-2}	[16]
Si/C/MnO_2	10	29.45 mF cm^{-2}	[17]
Au/B15C5$_{SAM}$	-	3.68 μF cm^{-2}	[18]
ITO/BENZ$_{10\ nm}$/Al	10	53 μF cm^{-2}	**This work**

16. Theoretical calculations

Table S14: Optimized calculations of total energy (Eh), zero point vibrational energy (kcal mol^{-1}), Rotational Constants (MHz), Entropy (kcal mol^{-1}), Dipole Moment (Debye), and HOMO–LUMO energy gap (eV) for 2,3 and 4 units of BENZ. A decrease in the HOMO-LUMO energy gap was consistent with an increase in the number

of BENZ units. However, in the actual system, the no. of BENZ layers is estimated at 41 but theoretically, it's not possible to consider such a bigger film.

Parameter	BENZ units		
	2	3	4
Total energy (Eh)	-1553.48	-2329.63	-3105.77
Zero point energy (Eh)	136.2	198.8	261.35
Rotational constants (MHz)	627.44	275.62	117.38
	125.51	41.05	20.72
	112.73	40.34	19.05
Entropy			
Total (kcal/mol)	38.23	49.26	58.69
Transational (kcal/mol)	12.81	13.17	13.43
Vibrational (kcal/mol)	15.02	24.82	33.31
Rotational (kcal/mol)	10.39	11.27	11.95
Dipole moment (μ)	8.58	13.50	16.90
HOMO–LUMO energy gap (Hartree)	0.237	0.234	0.228
HOMO–LUMO energy gap (eV)	6.449	6.367	6.204

17. References:

1 N. Singh, A. Malik, S. Nohwar, R. Jana and P. C. Mondal, *New J. Chem.*, 2023, **47**, 5308-5315.

2 R. Gupta, P. Jash, A. Pritam and P. C. Mondal, *Can. J. Chem.*, 2022, **100**, 530–537.

3 R. L. A.J. Bard, Faulkner, *Electrochemical Methods: Fundamentals and Applications*, John Wiley & Sons, Inc., New York, New York, 2nd edn., 2001.

4 Y. Chen, J. Yang, Z. Li, R. Li, W. Ruan, Z. Zhuang and B. Zhao, *Spectrochim. Acta - Part A Mol. Biomol. Spectrosc.*, 2016, **153**, 344–348.

5 J. Redolat, M. Camarena-Pérez, A. Griol, M. S. Lozano, M. I. Gómez-Gómez, J. E. Vázquez-Lozano, E. Miele, J. J. Baumberg, A. Martínez and E. Pinilla-Cienfuegos, *Nano Lett.*, 2024, **24**, 3670–3677.

6 A. Suwaiyan, R. Zwarich and N. Baig, *J. Raman Spectrosc.*, 1990, **21**, 243–249.

7 M. Gratzel, *nature*, 2001, **414**, 338–344.

8 W. P. Gomes and F. Cardon, *Prog. Surf. Sci.*, 1982, **12**, 155.

9 D. R. Chowdhury, L. Spiccia, S. S. Amritphale, A. Paul and A. Singh, *J. Mater. Chem. A*, 2016, **4**, 3655–3660.

10 V. Christou, M. Etchells, O. Renault, P. J. Dobson, O. V. Salata, G. Beamson and R. G. Egdell, *J. Appl. Phys.*, 2000, **88**, 5180–5187.

11 R. Andersson, A. M. Saleem and V. Desmaris, *Proc. - Electron. Components Technol. Conf.*, 2018, **May 29**, 2313–2318.

12 E. Hourdakis, I. Kochylas, M. A. Botzakaki, N. J. Xanthopoulos and S. Gardelis, *Solid. State. Electron.*, 2022, **196**, 108408.

13 M. F. El-Kady and R. B. Kaner, *Nat. Commun.*, 2013, **4**, 1475.

14 A. M. Saleem, R. Andersson, V. Desmaris and P. Enoksson, *Solid. State. Electron.*, 2018, **139**, 75–79.

15 Z. S. Wu, K. Parvez, X. Feng and K. Müllen, *Nat. Commun.*, 2013, **4**, 2487.

16 Z. S. Wu, Y. Z. Tan, S. Zheng, S. Wang, K. Parvez, J. Qin, X. Shi, C. Sun, X. Bao, X. Feng and K. Müllen, *J. Am. Chem. Soc.*, 2017, **139**, 4506–4512.

17 Y. Wang, L. Sun, D. Xiao, H. Du, Z. Yang, X. Wang, L. Tu, C. Zhao, F. Hu and B. Lu, *ACS Appl. Mater. Interfaces*, 2020, **12**, 43864–43875.
18 S. C. Patrick, R. Hein, P. D. Beer and J. J. Davis, *Chem. Sci.*, 2024, **15**, 18310–18317.